

1 **Salt thickness and composition influence rift structural style, northern North Sea, offshore Norway**

2
3 Christopher A-L. Jackson^{1*}, Gavin M. Elliott^{1‡}, Elisabeth Royce-Rogers^{1‡},
4 Rob L. Gawthorpe², Tor E. Aas³

5
6 ⁽¹⁾ *Basins Research Group (BRG), Department of Earth Science and Engineering, Imperial College,*
7 *Prince Consort Road, London, SW7 2BP, UK*

8
9 ⁽²⁾ *Department of Earth Science, University of Bergen, Allegate 41, N-5007 Bergen, Norway*

10
11 ⁽³⁾ *Statoil ASA, 4313 Sandnes, Norway*

12
13 ^(‡) *Now at: TGS, 1 The Crescent, Surbiton, Surrey, KT6 4BN, UK*

14
15 ^(*) *Now at: Lukoil Overseas UK Ltd, 5-11 Regents Street, London, SW1Y 4LR, UK*

16
17 **Corresponding author (e-mail: c.jackson@imperial.ac.uk)*

18
19 **ABSTRACT**

20
21 ‘Salt’ giants are typically halite-dominated, although they invariably contain other evaporite (e.g. anhydrite,
22 bittern salts) and non-evaporite (e.g. carbonate, clastic) rocks. Rheological differences between these rocks
23 mean they impact or respond to rift-related, upper crustal deformation in different ways. Our understanding
24 of basin-scale lithology variations in ancient salt giants, what controls this, and how this impacts later rift-
25 related deformation, is poor, principally due to a lack of subsurface datasets of sufficiently regional extent.
26 Here we use 2D seismic reflection and borehole data from offshore Norway to map compositional variations
27 within the Zechstein Supergroup (Lopingian), relating this to the structural styles developed during Middle
28 Jurassic-to-Early Cretaceous rifting. Based on the proportion of halite, we identify and map four intrasalt
29 *depositional zones* (*sensu* Clark et al., 1998) offshore Norway. We show that, at the basin margins, the
30 Zechstein Supergroup is carbonate-dominated, whereas towards the basin centre, it become increasingly
31 halite-dominated, a trend observed in the UK sector of the North Sea Basin and in other ancient salt giants.
32 However, we also document abrupt, large magnitude compositional and thickness variations adjacent to
33 large, intra-basin normal faults; for example, thin, carbonate-dominated successions occur on fault-bounded

34 footwall highs, whereas thick, halite-dominated successions occur only a few kilometres away in adjacent
35 depocentres. It is presently unclear if this variability reflects variations in syn-depositional relief related to
36 flooding of an underfilled presalt (Early Permian) rift or syn-depositional (Lopingian) rift-related faulting.
37 Irrespective of the underlying controls, variations in salt composition and thickness influenced the Middle
38 Jurassic-to-Early Cretaceous rift structural style, with diapirism characterising hangingwall basins where
39 autochthonous salt was thick and halite-rich, and salt-detached normal faulting occurring on the basin
40 margins and on intra-basin structural highs where the salt was too thin and/or halite-poor to undergo
41 diapirism. This variability is currently not captured by existing tectono-stratigraphic models largely based
42 on observations from salt-free rifts and, we argue, mapping of suprasalt structural styles may provide
43 insights into salt composition and thickness in areas where boreholes are lacking or seismic imaging is poor.

44

45 **INTRODUCTION**

46

47 The term ‘salt’ is typically used to describe halite-dominated rocks. However, ‘salt’ sequences may contain
48 other evaporite rocks such as anhydrite or, its hydrated form, gypsum, and non-evaporite rocks such as
49 carbonates and clastics (e.g. Warren, 2010, 2016; Hudec and Jackson, 2007; Jackson & Hudec, 2017).
50 These rocks have different mechanical properties and will accordingly show different styles of deformation
51 when stressed (i.e. faulting of carbonates and clastics, flow of halite). These variations in lithology and
52 mechanical properties, in addition to the bulk thickness of the salt and its overburden, are important to
53 consider when examining the structural evolution of rifts forming in crust containing thick salt sequences.
54 For example, the structural style and evolution of rifts containing relatively thick salt (e.g., Stewart et al.,
55 1996, 1997; Pascoe et al., 1999; Withjack and Callaway, 2000; Richardson et al., 2005; Stewart 2007; Kane
56 et al., 2010; Wilson et al., 2013; Rowan, 2014) differ significantly from salt-free rifts (e.g. Leeder and
57 Gawthorpe, 1987; Prosser, 1993; Gawthorpe and Leeder, 2000). These differences arise because salt
58 influences the degree and style of coupling between sub- and suprasalt deformation, and because activity
59 on sub- and suprasalt faults can trigger salt flow and halokinesis (Vendeville & Jackson, 1992; Jackson &
60 Vendeville, 1994). As a result, the physiography of and sediment dispersal patterns in, salt-influenced rifts
61 may be more complex than in salt-free rifts, thus questioning the general applicability of widely used rift
62 tectono-stratigraphic models (Gawthorpe and Leeder, 2000).

63 The Zechstein Supergroup is one of the world’s best-known and largest salt giants, documenting
64 repeated flooding and evaporation of a continent-scale saline water body that covered much of NW Europe
65 during the Lopingian (i.e. late Permian) (e.g. Glennie et al., 2003; Bachmann et al., 2010; Jackson &
66 Stewart, 2017; McKie, 2017; Soto et al., 2017). Notably, the Zechstein Supergroup occurs within the prerift

67 succession to and likely influenced the development of, the Middle Jurassic-to-Early Cretaceous rift. To-
68 date, most studies of Zechstein Supergroup compositional variations have focussed on the southern North
69 Sea and the north-western margin of the North Permian Basin (Fig. 1). For example, Clark et al. (1998),
70 using seismic reflection and very sparse borehole data from the north-western margin of the North Permian
71 Basin, demonstrate the Zechstein Supergroup is characterised by a thick sequence of halite and anhydrite
72 in the basin centre, and a relatively thin carbonate-clastic sequence at the basin margin (Figs 2 and 3). Based
73 on the overall thickness and seismic expression of the Zechstein Supergroup, and the approximate
74 percentage of halite, Clark et al. (1998) map four basin-scale *depositional zones* or ‘DZs’ (DZ1-4; see also
75 Taylor, 1990). DZ1, which contains <10% halite, occurs at the basin margin or on normal fault-bound,
76 intra-basin structural highs (Fig. 3). DZ2 (10-50% halite) and DZ3 (50-80% halite) occur on basinward-
77 dipping ramp-like areas, whereas DZ4 (>80 % halite), which constitutes the majority of the fill of the North
78 Permian Basin, occurs towards the basin centre (Fig. 3). It should be noted that, although elegant, the model
79 of Clark et al. (1998) is supported by only sparse borehole data

80 Compared to the UK sector, almost nothing is known about basin-scale compositional variations
81 in the Zechstein Supergroup in the Norwegian sector of the North Sea Basin (see Jackson & Stewart, 2017).
82 Jackson and Lewis (2016) use 3D seismic and reflection data from the Sele High Fault System, eastern Sele
83 High, to document rapid across-fault variations in salt thickness and composition, demonstrating the
84 footwall apex of this large-displacement fault system (>2 km) is capped by relatively thin (58 m), largely
85 immobile carbonate and claystone, whereas relatively thick (>200 m) and mobile halite occurs in the
86 adjacent hangingwall. The study of Jackson and Lewis (2016) covers only a relatively small area (*c.* 3600
87 km²) however, and to-date there has been no systematic regional study of basin-scale compositional
88 variability in the Zechstein Supergroup. Establishing this is important for two key reasons. First, given that
89 they appear directly related to syn-depositional basin structure, compositional variations may shed light on
90 the Lopingian physiography of the Norwegian sector of the North Permian Basin. More specifically, they
91 may reveal whether salt deposition occurred in a large unfaulted sag-like basin following an earlier period
92 of rifting, or in an active rift. Second, and because of variability in the mechanical properties of evaporite
93 and non-evaporite rocks, intra-Zechstein compositional variations may influence the structural style and
94 evolution of the Middle Jurassic-to-Early Cretaceous rift, which, at least in its southern reaches, developed
95 in the presence of salt.

96 We here use borehole data to map basin-scale (*c.* 30000 km²) variations in Zechstein Supergroup
97 composition on the north-eastern margin of the North Sea Basin. We also use long-offset, 2D seismic
98 reflection data to examine variations in Zechstein Supergroup thickness and geometry, and to constrain the
99 present sub- and suprasalt structure of the study area. By combining stratigraphic and structural data we are

100 able to investigate the role that composition variations in the Zechstein Supergroup had on the syn-rift
101 structural styles and evolution of the Middle Jurassic-to-Early Cretaceous rift system. We show that
102 compositional variations in the Zechstein Supergroup are strongly controlled by syn-depositional basin
103 relief; this relief may have been inherited from an earlier (i.e. presalt) tectonic event, or have formed during
104 salt deposition (i.e. synsalt). Furthermore, variations in salt composition and thickness strongly influenced
105 the Middle Jurassic-to-Early Cretaceous rift structural style; classic salt-tectonic, diapirism-dominated
106 structural styles form in areas where the autochthonous salt was thick and halite-rich, whereas salt-detached
107 normal faulting and only very minor diapirism occurs on the basin margins and on intra-basin structural
108 highs where salt is thin and/or halite-poor. Based on our findings, we suggest current rift basin tectono-
109 stratigraphic models need modifying to take into account the presence of pre-rift salt.

110

111 **TECTONO-STRATIGRAPHIC FRAMEWORK**

112

113 The study area is located in the Norwegian sector of the northern North Sea, with particular focus on the
114 South Viking Graben, Utsira High, Ling Depression and Egersund Basin (Fig. 1). Carboniferous-to-Early
115 Permian transtension drove initial normal fault-related basin subsidence and led to the formation of the
116 Egersund Basin, and the South Viking, Ling and Åsta grabens (Coward, 1995; Roberts *et al.*, 1995; Glennie,
117 1998; Coward *et al.*, 2003; Zanella and Coward, 2003). Following continental extension, Lopingian thermal
118 subsidence resulted in formation of the pan-European, North Permian Basin, which was subsequently
119 overprinted by the Middle Jurassic-to-Early Cretaceous rift-related basins listed above (Fig. 1A). The study
120 area lay towards the northern and north-western margins of the North Permian Basin (Fig. 1). A relative
121 sea-level rise in the earliest Lopingian established marine-to-marginal marine conditions in the North
122 Permian Basin, and repeated cycles of basin flooding and desiccation drove deposition of a >1 km thick,
123 evaporite-dominated unit (Zechstein Supergroup, herein referred to as ‘salt’; Figs 1 and 2). Previous studies
124 suggest that that the Zechstein Supergroup was up to 1.5 km thick in the South Viking Graben and Egersund
125 Basin, and indicate that carbonates and clastics at the basin margins pass basinwards into anhydrites and
126 halites in the basin axes (Pegrum and Ljones 1984; Sørensen *et al.*, 1992; Thomas and Coward 1996; Evans
127 *et al.*, 2003; Jackson *et al.* 2010; Jackson & Lewis, 2016).

128 The abundance of salt structures (e.g. pillows, diapirs) and rapid, large-magnitude variations in the
129 thickness of Triassic deposits confirms that post-depositional flow of Zechstein Supergroup salt occurred
130 in the South Viking and Ling Depressions during the Triassic (Pegrum and Ljones, 1984; Sørensen *et al.*,
131 1992; Erratt, 1993; Thomas and Coward, 1996, Jackson and Larsen, 2009; Kane *et al.*, 2010). In contrast,
132 the Åsta Graben, which likely contained thinner and/or less mobile evaporites, was less affected by salt

133 movement and was instead dominated by rift-related extension and faulting. In the Early Jurassic,
134 impingement of a mantle plume at the base of the lithosphere led to the formation of the Mid-North Sea
135 Dome, which drove transient uplift of much of the southern Viking Graben, the Moray Firth, and the north
136 and north-east Central Graben. Because of this major tectonic event, Triassic and older stratigraphic units
137 were locally completely eroded and Early Jurassic strata are locally absent due to non-deposition or erosion.
138 During the Middle to Late Jurassic, a combination of the collapse of the Mid-North Sea Dome and
139 extensional faulting led to flooding of the North Sea Rift System (Cockings *et al.*, 1992; Thomas and
140 Coward, 1996; Coward *et al.*, 2003; Lyngsie *et al.*, 2006).

141 Crustal extension during the Late Jurassic and Early Cretaceous reactivated many of the Permo-
142 Triassic, basement-involved normal fault systems bounding the main structural elements (e.g. the Graben
143 Bounding Fault Zone that bounds the western margin of the South Viking Graben; the Sele High and
144 Stavanger fault systems that bound the Egersund Basin and Åsta Graben; Lewis *et al.*, 2013; Jackson &
145 Lewis, 2016). Basement-involved faulting and tilting during the Late Jurassic and Early Cretaceous also
146 drove salt flow and the growth of diapirs, extension of supra-salt strata, and formation of salt-detached
147 (supra-salt) normal fault arrays (Thomas and Coward, 1996; Jackson and Larsen, 2009; Lewis *et al.*, 2013;
148 Tvedt *et al.*, 2013; Jackson and Lewis, 2016). Although some of the larger structures continued to be active,
149 many of the rift-related normal faults became inactive during the Late Cretaceous in response to declining
150 rates of crustal extension (Knott *et al.*, 1993; Thomas and Coward, 1996; Knott, 2001; Fraser *et al.*, 2003).
151 During the Late Cretaceous to Cenozoic, the Northern North Sea subsided due to cooling of the crust
152 following Late Jurassic-to-Early Cretaceous rifting; subsidence was, however, punctuated by a period of
153 inversion that resulted in squeezing and amplification of salt diapirs and local reverse reactivation of normal
154 faults (e.g. Biddle and Rudolph, 1988; Cartwright, 1989; Sørensen *et al.*, 1992; Fraser *et al.* 2003; Jackson
155 *et al.*, 2013).

156

157 **DATASET AND METHODS**

158

159 This study integrates wireline log data from 22 wells and 2D seismic reflection profiles covering Norwegian
160 North Sea exploration blocks 8-10, 16-18 and 25 (Fig. 1). The seismic profiles are spaced every c. 5 km in
161 the south-east and c. 10 km in the north-west of the study area. The seismic data are time-migrated and are
162 presented in two-way time (TWT). The record length is 9 sec TWT, which is sufficient for imaging subsalt
163 units across much of the basin. The heights of halite-rich salt structures (e.g. diapirs) are calculated using
164 an interval velocity for salt of 4500 m/s⁻¹. All profiles are displayed with ‘normal’ polarity (i.e. an increase
165 in acoustic impedance with depth is represented by peak or black reflection, whereas a decrease in acoustic

166 impedance with depth is represented by trough or red reflection; see Brown, 2004). Twenty-two exploration
167 wells, which fully or partially penetrate the Zechstein Supergroup, allow a petrophysical characterisation
168 of the key lithologies within the Zechstein Supergroup and regional and local mapping of these units (Fig.
169 1 and Table 1). Key lithostratigraphic or chronostratigraphic surfaces were identified in wells and tied to
170 the seismic data. Five regionally correlatable seismic horizons were interpreted: (i) top Rotliegend Group
171 (top middle Permian); (ii) top Zechstein Supergroup (top Permian); (iii) top Hegre Group (approximate top
172 Triassic); (iv) top Viking/Boknfjord Group (top Jurassic); and (v) top Shetland/Chalk Group (top
173 Cretaceous) (Fig. 2). Based on the distribution of seismic and well data we define two main study areas; a
174 northern area that focuses on the South Viking Graben, Utsira High and Sleipner Terrace, and a southern
175 area focused on the Ling Depression, Sele High and Egersund Basin (Fig. 1).

176 To identify evaporite and non-evaporite lithologies in the Zechstein Supergroup we combined
177 observations from wireline petrophysical logs and cuttings data (from well reports and composite logs)
178 from 10 of the 22 wells. Cuttings data were used to identify the principal Zechstein Supergroup lithologies,
179 whose petrophysical expression was then constrained by extracting corresponding log values at 1, 10 and
180 20 m intervals, depending on unit thickness (i.e. 0-500 m, 500-1000 m and >1000 m thick respectively). A
181 total of 1307 points were extracted and used to create cross-plots (i.e. sonic velocity vs. density; GR vs.
182 sonic velocity); these cross-plots defined petrophysical ranges for each lithology that then allowed us to
183 interpret lithology variations from wireline logs in wells (or sections of wells) lacking cuttings data (see
184 next section). We then defined seven lithologies or ‘petrophysical facies’: (i) anhydrite; (ii) halite; (iii)
185 carnallite (i.e. a mineral consisting of a hydrated potassium or magnesium chloride); (iv) ‘carbonate’
186 (dolomite and limestone); (v) shale-claystone; (vi) siltstone, and (vii) sandstone (Fig. 4 and Table 2).

187 Regional stratigraphic correlations based on well data and tied to regional seismic reflection
188 profiles were then constructed to examine the lateral variation in Zechstein Supergroup lithology and
189 thickness. These combined well log/seismic stratigraphic correlations allowed the structural context of
190 individual wells to be identified (i.e. whether a well is located in the basin centre, at the basin margin, on
191 an intra-basin structural high, in a major salt structure, etc; Table 1). However, due to a lack of
192 biostratigraphic data and because of substantial post-depositional salt flow, it is not possible to correlate
193 individual, metre- to decametre-scale, evaporite or non-evaporite stratigraphic packages within the
194 Zechstein Supergroup. We acknowledge that post-depositional salt flow likely resulted in some tectonic
195 modification of the primary depositional stratigraphy due to preferential expulsion of more mobile
196 lithologies (e.g. halite and carnallite; “*tectonic purification by movement*”; *sensu* Kupfer, 1968; see also
197 Hudec and Jackson, 2007; Cartwright et al., 2012; Jackson et al., 2014a). For example, a well may be halite-
198 poor simply because halite flowed into and inflated flanking diapirs; in this case, this well will be

199 erroneously assigned to DZ1 or 2 and not DZ3 or 4. However, we argue our seismic reflection and well
200 data provide an acceptable record of the primary lithology distribution within the Zechstein Supergroup;
201 more specifically, areas dominated by thick, halite-dominated sequences are characterised by diapirs,
202 whereas those characterised by thin, halite-poor sequences lack such structures. Furthermore, to help us
203 assign individual wells to specific depositional zones, we use seismic reflection data to provide structural
204 context to each well; i.e. does it lie within an area lacking any evidence for salt movement (in which case
205 it likely lies within DZ1 or 2), or does it penetrate an area of pronounced diapirism, and if so, is it within
206 the core of a diapir or in a flanking area of thin salt (in which case it likely lies within DZ3 or 4) (see Table
207 1).

208

209 **PETROPHYSICAL EXPRESSION OF THE ZECHSTEIN SUPERGROUP**

210

211 Density (RHOB)-sonic velocity (DT) cross-plots were used to differentiate between halite and anhydrite;
212 halite has relatively low density (1.9-2.3 g/cm³) and moderate velocity (65-73 µs/ft), whereas anhydrite has
213 relatively high density (typically 2.7-3.1 g/cm³) and very high velocity (typically 49-58 µs/ft) (Fig. 4; Table
214 2). Overlap of the anhydrite and carbonate fields on RHOB-DT cross-plots suggests the anhydrite may be
215 impure, although the former is identified based on its much lower velocity (<55 µs/ft) and slightly higher
216 density (>2.8 g/cm³) (Fig. 4). Carbonate and clastic (especially claystone) rocks overlap in terms of these
217 density (2.3-2.9 g/cm³), velocity (48-90 µs/ft) and radioactivity (10-250 API), although siltstone/sandstone
218 typically has overall lower velocity (typically >75 µs/ft) and radioactivity (35-60 API). It is therefore
219 impossible to discriminate between carbonate and claystone in wells (or sections of wells) lacking cuttings
220 (Figs 4 and 5; see also Table 2). More generally, the highly variable and overlapping petrophysical
221 characteristics of the carbonate and clastic lithologies suggest they were incorrectly identified in cuttings
222 data, or that they are impure, containing a mixture of, for example, anhydrite and claystone (i.e. a 'dirty
223 anhydrite') or sandstone and carbonate (i.e. 'sandy carbonate'). Carnallite is relatively rare in the Zechstein
224 Supergroup and thus infrequently sampled in cuttings. As a result, this lithology is identified in wells based
225 on higher radioactivity (0-50 API), lower density (2-2.2 g/m³), and higher velocity (58-70 µs/ft) values than
226 other evaporite lithologies (i.e. halite and anhydrite; Table 2). Despite the limitations of our wireline log-
227 based analysis, we feel it provides a good first-order assessment of lithology variations in the Zechstein
228 Supergroup. More specifically, these data allow us to discriminate between evaporite and non-evaporite
229 lithologies; this is a crucial distinction, given the amount of evaporite ultimately governs the mobility of
230 the Zechstein Supergroup, and the structural style and evolution of the rift.

231

232 **DISTRIBUTION, THICKNESS, LITHOLOGY AND STRUCTURE OF THE ZECHSTEIN** 233 **SUPERGROUP**

234

235 A regional two-way time (TWT) thickness (isochron) map shows that the Zechstein Supergroup is typically
236 c. 200 ms (c. 450 m) thick, but is up to 1000 ms (c. 2250 m) thick in diapirs located in the axes of the major
237 fault-bound depocentres (e.g. the Ling Depression, where diapirs are penetrated by 16/11-1S and 16/8-2;
238 Fig. 6; see also seismic profiles in Figs. 7-10). Towards the eastern margin of the South Viking Graben the
239 Zechstein Supergroup is relatively thin (<100 ms TWT; c. 225 m) and salt structures are sparse. The
240 Zechstein Supergroup is also thin on intra-basin structural highs such as Sele High (<60 m; 17/12-2) and
241 Sleipner Terrace (<100 m; 16/1-2). Seismic data thus suggest a first-order positive relationship between the
242 present thickness and mobility of the Zechstein Supergroup (e.g. thick Zechstein Supergroup is mobile; thin
243 Zechstein Supergroup is immobile; Jackson & Lewis, 2016). Furthermore, basement-involved normal faults
244 appear to exert a primary control on the Zechstein Supergroup thickness, with the unit being thinnest on
245 basin margin or intra-basin, fault-bound structural highs (e.g. Sele High and flanks of Utsira High), and
246 thickest in deep basins such as the Ling Depression (Fig. 6). Below we describe the thickness and
247 composition of the Zechstein Supergroup in three sub-areas, and assign individual wells to specific salt-
248 related depositional zones. We then relate these salt-related depositional zones to the styles of salt-diapirism
249 and rift-related deformation.

250

251 **Sub-area 1: South Viking Graben, Sleipner Terrace and Utsira High**

252

253 The correlation panel in Figure 7 illustrates variations in thickness and lithology of the Zechstein
254 Supergroup between relatively deep depocentres such as the South Viking and Ling Depressions, and
255 relatively shallow, basin margin locations such as the western margin of the Utsira High and the Sleipner
256 Terrace. Four wells (15/5-3, 16/4-1, 15/9-9 & 15/12-3) on this panel penetrate the entire Zechstein
257 Supergroup succession, whereas 15/12-2 only penetrates its upper 37 m. Wells located in the axis of the
258 South Viking Graben (15/5-3) and Ling Depression (15/12-3) penetrate diapirs and indicate that the
259 Zechstein Supergroup, which in well 15/5-3 is up to 1046 m thick, is dominated by halite (93% of the
260 penetrated thickness) with relatively thin (<30 m) intervals of anhydrite and more rarely, carnallite. Using
261 the scheme of Clark et al. (1998), 15/5-3 lies in DZ4. In the axis of the Ling Depression the Zechstein
262 Supergroup is 1203 m thick, with the upper 743 m being halite-dominated and containing thin (<5 m)
263 carnallite layers (15/12-3; Fig. 7A). The lower 260 m of the succession is claystone-dominated, with
264 relatively thin (<30 m) anhydrite and halite intervals. Overall, 15/12-3 comprises >70% halite and it

265 therefore lies within DZ3. Seismic data indicate that, in these deep basin locations, where the Zechstein
266 Supergroup is relatively thick and halite-dominated (i.e. DZ3-4), large diapirs occur (Figs 7B). Thinning
267 and onlap of the Triassic succession across these salt structures suggests salt flow occurred during the
268 Triassic; a later period of flow during the Middle to early Late Jurassic is also locally indicated by thinning
269 and onlap of the corresponding interval across some of the salt-cored structures (Fig. 7). 15/12-2, despite
270 being anhydrite-dominated, is assigned to DZ3, given it penetrates the only the crest of a moderate-relief
271 (c. 500 ms TWT; c. 1125 m) diapir, the presence of which indicates the Zechstein Supergroup is relatively
272 thick and mobile in this location (Fig. 7). We infer the anhydrite represents part of the diapir caprock (e.g.
273 Warren, 2016).

274 In contrast to the deep basin wells, 16/4-1 and 15/9-9, which are located on present-day structural
275 highs defining the basin margins, contain a relatively thin, halite-poor Zechstein Supergroup (Fig. 7). In
276 16/4-1, located on the western margin of the Utsira High, the Zechstein Supergroup is dominated by clastic
277 lithologies (siltstone and sandstone) with only minor anhydrite and carbonate. Likewise, 15/9-9, located on
278 the Sleipner Terrace, is largely composed of anhydrite with minor carbonate; halite is lacking. The halite-
279 poor nature of these wells places both of these wells and the domains they represent within DZ1. Seismic
280 data indicate that at the basin margins, where the Zechstein Supergroup is relatively thin and halite-poor
281 (i.e. DZ1), salt structures are very rare, with very little relief being developed at top salt (Fig. 7B).

282 A correlation panel along the western flank of the Utsira High further illustrates the variations in
283 thickness and lithology occurring in the Zechstein Supergroup at the basin margin (Fig. 8). Four wells
284 completely penetrate a relatively thin (<150 m) Zechstein Supergroup succession, but only 16/1-2 and 16/7-
285 2 occur close to seismic reflection profiles (Fig. 8). All of the wells lack halite and are dominated by non-
286 evaporitic lithologies such as carbonate, fine-grained clastics and anhydrite. In the most northern well,
287 evaporite facies are completely absent and the Zechstein Supergroup is composed only of claystone and
288 carbonate (25/10-4R). Well 25/10-2R, which is located on the western flank of the Utsira High, is
289 carbonate-rich (50%), particularly towards its base, but it also contains anhydrite with a thin shale-claystone
290 layer at the top of the Zechstein Supergroup. Well 16/1-2, is also carbonate-dominated, although anhydrite
291 occurs in the middle of the Zechstein Supergroup and claystone is found towards its top and base (Fig. 8).
292 The upper and lower parts of the Zechstein Supergroup in well 16/7-2, located at the southern tip of the
293 Utsira High, are carbonate-rich, although anhydrite and shale-claystone are prevalent in the middle part of
294 the well. Based on their lack of halite, wells along the flanks of the Utsira High are representative of DZ1.
295 As we observed for the south-western Utsira High and the Sleipner Terrace: (i) salt structures are absent on
296 the basin margins where the Zechstein Supergroup is relatively thin and halite-poor (i.e. DZ1); and (ii)

297 basement-involved faults locally cross-cut halite-poor Zechstein Supergroup, extending up into the
298 Mesozoic succession (Fig. 8B). We discuss the significance of these two observations below.

299

300 **Sub-area 2: Ling Depression, Sele High and Åsta Graben**

301

302 Two broadly E-trending correlation panels illustrate the variations in Zechstein Supergroup thickness and
303 lithology occurring between the present basin margins (i.e. Sleipner Terrace) and intra-basin highs (i.e. Sele
304 High; Fig. 9), and the adjacent fault-bound depocentres (i.e. Ling and Åsta grabens; Fig. 10). Beginning
305 with the most northerly of these two panels (Fig. 9), our data show that, on the Sleipner Terrace, the
306 Zechstein Supergroup is 25–64 m thick and it is notable for its lack of halite. Instead, the Zechstein
307 Supergroup is dominated by anhydrite (74%; 15/9-16) or claystone (48%; 16/7-3), with moderate amounts
308 of carbonate (26-27% in 15/9-16 and 16/7-3). The Zechstein Supergroup succession is thus compositionally
309 similar to that encountered along the eastern flank of the South Viking Graben, on the margin of the Utsira
310 High (cf. Fig. 8). 16/8-2 and 16/9-1, which are located within the Ling Depression only 17 km to the east
311 of 16/7-3, are separated from the Sleipner Terrace by a south-eastward dipping, NE-SW-striking normal
312 fault that has 660 ms of throw at top Rotliegend Group level (Figs. 1 and 9B). In the hangingwall of the
313 fault system, 16/8-2 penetrated a salt wall at least 1325 m thick and comprising 94% halite with minor
314 amounts of anhydrite, carbonate and carnallite; the Zechstein Supergroup in this location can be included
315 in DZ4. Well 16/9-1, which is also located on the western flank of the Sele High, only penetrated the upper
316 140 m of a c. 450 m thick Zechstein Supergroup succession, with the penetrated interval dominated by
317 anhydrite (63%), although halite is present (35%), together with a thin (<10 m) claystone unit cap (Fig. 9).
318 Based exclusively on the lithologies encountered in its upper part, the Zechstein Supergroup in this well is
319 assigned to DZ3. Seismic data indicate again that structural style is closely coupled to Zechstein Supergroup
320 thickness and composition; on the basin margins, where the unit is thin and halite-poor (i.e. DZ1-2), no salt
321 structures or only very low-relief pillows occur, with normal faults cross-cutting the salt and extending
322 from subsalt into suprasalt strata (i.e. Sele High and Sleipner Terrace; Fig. 9B). In contrast, in the basin
323 centre, where the unit is thick and halite-rich (i.e. DZ3-4), diapirs are common (i.e. Ling Depression; Fig.
324 9B). Supra-salt, salt-detached normal faults, which extend up into Tertiary strata, are also developed in
325 basin centre locations (Fig. 9B).

326 The southerly of the two panels further highlights the lateral lithology and thickness variations
327 occurring in the Zechstein Supergroup between intra-basin, fault-bound highs and adjacent depocentres
328 (Fig. 10). 16/10-1, 16/11-1S and 17/11-1 are located within the Ling Depression and, although none of
329 these wells penetrate the entire thickness of the Zechstein Supergroup, through the use seismic data it is

330 possible to constrain the approximate thickness of the Zechstein Supergroup at each well location by
331 projecting the wells onto the seismic data. This exercise suggests 16/10-1 penetrates the upper 35 m of a
332 salt wall that is *c.* 315 m thick (Fig. 10A). Wireline-log data suggest the Zechstein Supergroup is dominated
333 by halite (66%), with anhydrite, claystone and rare carnallite occurring in the upper few tens of metres
334 (DZ3). 16/11-1S also penetrates a salt wall, with seismic data suggesting the Zechstein Supergroup in this
335 location is *c.* 820 m thick (Fig. 10). The upper 794 m of the Zechstein Supergroup is penetrated in this well,
336 with wireline-log data indicating it is composed almost entirely of halite (99%) with minor amounts of
337 anhydrite and carbonate in the upper 38 m (DZ4). 17/11-1 in the Ling Depression penetrates the Zechstein
338 Supergroup in an area that appears to have undergone relatively limited amounts of post-depositional salt
339 flow. The well penetrates a 755 m thick succession of the Zechstein Supergroup, with seismic data
340 suggesting a further *c.* 15 m of Zechstein Supergroup occurs beneath the base of the well. In this location
341 the Zechstein Supergroup is dominated by halite (78%), with carnallite and carbonate-rich intervals
342 occurring in the lower 50 m, and anhydrite and carbonate-rich intervals occurring in the upper 20 m (Fig.
343 10). Decimetre-thick carbonate intervals also occur in the upper third of the unit. Based on these bulk
344 lithological variations, the Zechstein Supergroup in this location is assigned to DZ3. 17/12-2, which is
345 located 22 km updip to the east of 17/11-1, on the eastern margin of the Sele High, in the immediate footwall
346 of the Sele High Fault System, fully penetrates a thin (49 m), carbonate-dominated (84%) Zechstein
347 Supergroup (DZ1). 17/12-1R, which is located 15 km to the east of 17/12-2 and in the hangingwall of the
348 Sele High Fault System, penetrates the upper 100 m of a 450 ms TWT (*c.* 1013 m) thick salt pillow (Fig.
349 10B; see also Jackson & Lewis, 2015). The Zechstein Supergroup in the well is composed predominantly
350 of halite (69%), although the upper 27 m is dominated by anhydrite and claystone; by assuming the salt
351 pillow below the termination of the well is halite-dominated, we tentatively place 17/12-1R in DZ4 (Fig.
352 10). We interpret the 27 m thick anhydrite and claystone-rich unit capping the pillow represents caprock
353 (e.g. Warren, 2016).

354 When considering the salt- and rift-related structural styles we note that large Triassic-to-Jurassic
355 minibasins are flanked by diapirs in the basin centre and on the lower flanks of intra-basin highs where the
356 Zechstein Supergroup is thick and halite-rich (i.e. DZ3-4) (i.e. Ling Depression; Fig. 10B). On crests of
357 intra-basin fault-bound highs, where the unit is thin and halite-poor (i.e. DZ1-2), no large salt structures
358 occur, although small rollers are present in the footwalls of salt-detached faults (i.e. Sele High; Fig. 10B).
359 However, downdip of structural culminations such as the Sele High, in areas ascribed to DZ2 and 3 (i.e.
360 10-80% halite), seismic data image a range of salt-related structures including diapirs, minibasins and rafts
361 (Figs 11, 12, and 13).

362

363 **Sub-area 3: Egersund Basin and Lista Nose**

364

365 A correlation panel (Fig. 14) covering the south-eastern part of the Egersund Basin and the north-eastern
366 edge of the Lista Nose illustrates lithological variations in the Zechstein Supergroup immediately adjacent
367 to the Stavanger Platform. Based on the lithology of the Zechstein Supergroup sampled by wells in this
368 location, the Zechstein Supergroup has been assigned to DZ1 (i.e. 10/7-1 and 10/5-1) and 3 (i.e. 10/8-1).
369 For example, 10/7-1, located on the eastern edge of the Egersund Basin, appears to sample the upper 45 m
370 of a diapir flank. The well lacks halite and is composed solely of non-evaporitic lithologies; the lower part
371 of the well is clastic-dominated whereas the upper part of the well is dominated by carbonate (Fig. 4).
372 Again, because 10/7-1 only penetrates the upper part of the salt, assigning a depositional zone is not
373 straightforward, with the well penetrating the upper part of a large (1500 ms TWT; 667 m tall) diapir
374 developed above a horst (Fig. 14). As such, we infer that well samples caprock, and potentially straddles
375 the boundary between an area of thick, mobile salt to the SW in the Egersund Basin and thinner, slightly
376 less mobile salt to the NE on the Lista Fault Blocks. We suggest the diapir was thus either fed by mobile
377 salt expelled from the hangingwall during rifting (cf. Dooley et al., 2005; Burliga et al., 2012), or that the
378 whole area, including the horst, was characterised by relatively thin but still mobile salt, with the sub-salt,
379 basement-involved faults forming later and offsetting the base of the salt. 10/8-1, which is situated on the
380 Lista Nose, penetrates the upper part of a salt pillow and indicates the Zechstein Supergroup is composed
381 of anhydrite (12%) and claystone (22%) that overlie a halite-rich (66%) succession (DZ3). Finally, in 10/5-
382 1, which is located near the boundary between the Lista Nose and the Stavanger Platform (Fig. 1), and
383 which appears to penetrate the lower flank of moderately large (500 ms TWT) diapir, the Zechstein
384 Supergroup is 217 m thick and lacks halite. Instead, a 138 m thick, carbonate-rich succession overlies an
385 anhydrite and marl-rich unit that is underlain by a clastic-rich unit defining the base of the Zechstein
386 Supergroup (DZ1). Given the lack of halite, the Zechstein Supergroup should not be mobile in this location,
387 suggesting: (i) the well, which is projected 1175 m onto the seismic profile in Fig. 14, actually lies on a
388 structural high that lies away from this profile (see Fig. 1); or (ii) the well does indeed intersect a diapir,
389 but that it penetrates an area where halite has been preferentially expelled into the flanking diapir (e.g.
390 Kupfer, 1968; Hudec and Jackson, 2007; Cartwright et al., 2012; Jackson et al., 2014a).

391

392 **INTERPRETATION AND DISCUSSION**

393

394 **Controls on Zechstein Supergroup thickness and compositional variations in the northern North Sea**

395

396 Well and 2D seismic reflection data have allowed us to define the present thickness and lithological
397 variations in the Zechstein Supergroup along the northern margin of the North Permian Basin, offshore SW
398 Norway. These data indicate that the Zechstein Supergroup is relatively thin (<200 m) and halite-poor (i.e.
399 DZ1 and 2) at the basin margins and on normal-fault bound, intra-basin structural highs (e.g. Sele High);
400 in these locations the unit is dominated by anhydrite and non-evaporitic lithologies such as claystone,
401 carbonate and siltstone. In contrast, the Zechstein Supergroup is relatively thick (>200 m) and halite-rich
402 (i.e. DZ3 and 4) in the relatively deep, normal fault-bound basins (e.g. Ling Depression, Egersund Basin
403 and the axis of the South Viking Graben); in these locations, anhydrite and claystone only occur as part of
404 caprock sequence. Changes in lithology across basement-involved normal faults can be relatively abrupt
405 (e.g. between the Sleipner Terrace and the Ling Depression; Fig. 9; between the Sele High and the Egersund
406 Basin; Figs 7 and 15), or gradational (e.g. between the South Viking Graben and Utsira High; Fig. 7).
407 Moderately halite-rich parts of the Zechstein Supergroup (DZ2 and 3) occur in transitional areas, such as
408 fault-bound, basin-margin terraces or on largely unfaulted, gently basinward-dipping ramps (e.g. western
409 margin of the Utsira High).

410 Similar relationships between thickness, composition, and structural position have been described
411 from the UK sector of the North Sea (Fig. 3; Clark et al., 1998; Stewart, 2007; see also Jackson and Lewis,
412 2013 and Jackson & Stewart, 2017); we incorporate these observations with our data from offshore SW
413 Norway to produce what we believe is the first, almost fully northern North Sea-wide map of the Zechstein
414 Supergroup distribution and lithology (Fig. 15). Even though the relationship between Zechstein
415 Supergroup thickness and composition, and structural position is strong, it is not clear if the thickness, and
416 potentially, the primary lithological variability of the unit has been strongly modified by post-depositional
417 flow; in this case, unit thickness and composition may not, therefore, reflect or be used to infer the syn-
418 depositional basin physiography. For example, does thinning of the Zechstein Supergroup onto the
419 basement margins reflect a primary depositional pinchout or merely an erosional boundary related to post-
420 depositional erosion/dissolution? Related to this, does the thin/halite-poor nature of the Zechstein
421 Supergroup at the basin margins and on intra-basin structural highs, and the thick/halite-rich nature of the
422 unit of the unit in the basin centre, reflect a eustatic control on deposition (see Tucker, 1991), or simply the
423 impact of post-depositional tectonics and erosion on preservation and composition?

424 We propose that one or a combination of the four following end-member models may account for
425 the thickness and lithology variations observed in the Zechstein Supergroup (Fig. 16; see also Jackson and
426 Lewis, 2013): (i) *Model 1* (Fig. 16a) - the Zechstein Supergroup was deposited within a largely unstructured,
427 bowl-shaped basin and was halite-rich across the entire basin, including the basin margins and the future
428 positions of intra-basin structural highs. Post-depositional uplift associated with subsequent Triassic and/or

429 Middle Jurassic-to-Early Cretaceous rifting resulted in erosion and dissolution of the halite components of
430 the Zechstein Supergroup, and the relative enrichment in non-halite lithologies at the basin margins and on
431 intra-basin structural highs. Erosion, dissolution and relative enrichment of the Zechstein Supergroup in
432 anhydrite may also have occurred in response to exposure of the Zechstein Supergroup at the flexural rather
433 than fault-bound basin margins of the North Permian Basin during Triassic exposure; (ii) *Model 2* (Fig.
434 16b) – the Zechstein Supergroup was deposited in a largely unstructured, bowl-shaped basin and was
435 characterised by gradual changes in thickness and lithology, with halite- and carnallite-poor successions at
436 the basin margin passing gradually basinwards into halite-rich successions in the basin centre (e.g. Clark et
437 al., 1998; Stewart, 2007). Post-depositional flow of the Zechstein Supergroup was, however, strongly
438 partitioned, with mobile halite being preferentially expelled from the source layer on the basin margin into
439 flanking salt structures, resulting in local enrichment of non-halite lithologies in areas where the Zechstein
440 Supergroup is thin. This model applies not only to areas where salt is thin due to the subsalt basin structure,
441 but also due to welding due to post-depositional flow (Kupfer, 1968; Wagner and Jackson, 2011; Jackson
442 et al., 2014); (iii) *Model 3* (Fig. 16c) - the Zechstein Supergroup was deposited in a bathymetrically complex
443 basin, the physiography of which was inherited from the Early Permian rift event. Flooding of the basin by
444 the Zechstein Sea during the Lopingian resulted in halite deposition in high accommodation areas (e.g.
445 underfilled basin centre) during sea-level lowstand and carbonate/anhydrite deposition in low
446 accommodation areas (e.g. overfilled basin margin) during sea-level highstand (cf. Tucker, 1991). In this
447 model, subaerial exposure of the Zechstein Supergroup at the basin margin or on intra-basin structural highs
448 during the Triassic or Middle Jurassic-to-Early Cretaceous may have slightly modified the primary
449 lithology and thickness variations in the unit; and (iv) *Model 4* - the Zechstein Supergroup was deposited
450 in a bathymetrically complex basin, the physiography of which was controlled by syn-depositional (i.e.
451 Lopingian) rift-related normal faulting. In a similar manner to *Model 3*, *Model 4* envisages that halite was
452 deposited in high-accommodation areas during sea-level lowstand and carbonate/anhydrite deposition
453 occurred in low-accommodation areas at the basin margin during sea-level highstands (cf. Tucker, 1991).
454 In this model, variations in the thickness and lithology of the Zechstein Supergroup were simply augmented
455 by syn-depositional faulting (not shown in Fig. 16c).

456 Although post-depositional erosion and dissolution (*Model 1*) undoubtedly impacted on the present
457 thickness and lithology variations in the Zechstein Supergroup, we think it was unlikely to be the dominant
458 control because many of the basin-centre successions contain almost no carbonate and, even when relatively
459 thick salt is almost fully penetrated, relatively little anhydrite (e.g. 15/5-3; Fig. 7; 16/8-2; Fig. 9). This
460 suggests that the successions encountered at the basin margins or on intra-basin structural highs cannot
461 simply represent anhydrite- or carbonate-enriched versions of the basin-centre successions. We also

462 discount preferential flow of halite as being the dominant control on the lithological variations in the
463 Zechstein Supergroup because the thin successions encountered on the basin margin and intra-basin
464 structural highs are not flanked by large salt structures (e.g. 15/9-9 and 16/4-1; Figs 7 and 9). Although
465 Jackson and Lewis (2013) provide evidence for Early Permian rifting and faulting along at least the northern
466 margin of the Egersund Basin, and despite dramatic changes in thickness and lithology occurring in the
467 Zechstein Supergroup across basement-involved normal faults, we have no independent evidence for a
468 regional phase of Lopingian extension, thus making it difficult to discriminate between Models 3 and 4.

469

470 **Mechano-stratigraphic controls on structural style development in salt-influenced rift basins**

471

472 Salt has unique rheological properties, being weak under both extension and compression and, most
473 importantly. It is weaker than most other lithologies at significant (>500 m) burial depths and flows like a
474 fluid over geological timescales (e.g. Hudec and Jackson, 2007; Jackson and Hudec, 2017). As a result of
475 these rheological properties, salt can strongly modify the structural style of rift basins (e.g. Stewart et al.,
476 1996, 1997; Clark et al., 1998; Duffy et al., 2013; Wilson et al., 2013; Jackson & Lewis, 2016). For example,
477 salt can impede the vertical (and lateral) propagation of faults, and thus degree of sub- and supra-salt
478 kinematic coupling. Furthermore, activity on basement-restricted, thick-skinned and supra-salt faults can
479 trigger halokinesis by, for example, tilting the salt and triggering thin-skinned, gravity-driven deformation
480 and causing reactive diapirism (e.g. Vendeville and Jackson, 1992). As a result, the structural style of salt-
481 influenced rifts is markedly different to rifts that lack salt in their pre-rift mechano-stratigraphic template.

482 Here we have shown that spatial variations in the thickness and lithology of the evaporite-bearing
483 Zechstein Supergroup control the structural styles that develop during Middle Jurassic-to-Early Cretaceous
484 rifting (see also Lewis et al., 2013; Jackson and Lewis, 2016). Diapirism is common in hangingwall basins,
485 where autochthonous salt was thick and halite-rich (e.g. DZs 3 and 4 of Clark et al., 1998). In contrast, at
486 the basin margins and on intra-basin structural highs, in locations where the Zechstein Supergroup was too
487 thin and/or halite-poor to form large diapirs, salt-detached normal faulting occurs in response to basement-
488 involved faulting and structural tilting of top salt (e.g. DZs 1 and 2 of Clark et al., 1998). Locally, very
489 small minibasins may form, although these are rare. This variability is currently not captured by existing
490 tectono-stratigraphic models largely based on observations from salt-free rifts (Gawthorpe and Leeder,
491 2000). As a corollary, mapping of supra-salt structural styles may provide insights into salt lithology and
492 thickness in areas where boreholes are lacking or seismic imaging is poor below thick, structurally complex
493 overburden. Our study lends support to the UKCS-derived models of Clark et al. (1998) and Stewart (2007),
494 which are based on sparse, low-to-moderate quality 2D seismic data, and even sparser well controls.

495 The thickness and composition of the Zechstein Supergroup also impact the degree of sub- and
496 supra-salt kinematic coupling. For example, where it is thin and halite-poor near marginal or intra-basinal
497 structural highs, basement-involved normal faults cross-cut the unit and extend up into the Mesozoic, and
498 sometimes, Cenozoic successions (e.g. Utsira High; Fig. 8). In contrast, where it is thick and halite-rich,
499 the Zechstein Supergroup effectively decouples deformation, with the upper tips of the basement-involved
500 normal faults being confined to the thick, diapiric salt layer (e.g. Ling Depression; Fig. 9).

501

502 **Comparison to other saline giants**

503 Very few studies have documented the lithological variations occurring in ‘salt giants’ (*sensu* Hsü, 1972);
504 this may reflect a lack of borehole data with which to directly constrain such variations, or a lack of detailed
505 study on the evaporite-dominated stratigraphic interval in those particular basins. Where borehole data are
506 available, they indicate that lithology variations are strongly linked to the pre- or syn-depositional
507 physiography of the salt basin. For example, the middle Carboniferous-to-Permian, Paradox Basin, Utah,
508 USA is a large (265 km by 190 km), asymmetric, foreland basin that formed during the ancestral Rocky
509 Mountain orogenic event. Thrust sheet loading and long-wavelength crustal flexure led to the formation of
510 a gently north-eastwards dipping homocline, onto which a thick, evaporite-bearing sequence was deposited
511 (Paradox Formation; e.g. Barbeau, 2003; Trudgill *et al.*, 2004; Matthews *et al.*, 2007; Trudgill, 2011).
512 Because of the relatively simple basin geometry, somewhat predictable lithological and structural style
513 variations occur. In the basin centre the Paradox Formation is halite-rich, although potash, anhydrite and
514 organic-rich black shales occur. Together, these units are arranged into 29 evaporite-shale cycles
515 documenting periodic flooding and desiccation of the basin (Baars, 1983). In contrast, towards the basin
516 margins, the percentage of halite in the Paradox Formation decreases and the succession becomes
517 dominated by carbonates. Seismic reflection data indicate that the style of salt structures in the Paradox
518 Basin reflect this lateral variation in lithology and inferred rheology of the ‘salt’. For example, large salt
519 diapirs characterise the halite-rich, basin centre locations, whereas the basin margin is relatively
520 undeformed. A similar overall relationship between basin morphology, lithology variations, and structural
521 style are observed in the Santos Basin, offshore Brazil (e.g. De Freitas, 2006; Moreira *et al.*, 2007; Gamboa
522 *et al.*, 2008) and in the Mid-Polish Trough, Poland (e.g. Krzywiec, 2012).

523 Our study from the Norwegian sector of the North Sea Basin indicates that lithology and structural
524 style variations are more complex in salt basins characterised by rapid changes in syn-depositional basin
525 relief and eustatic sea-level variations. More specifically, the length-scales of lithology and thus structural
526 style change are much shorter (<1 km) in rift basins (e.g. the Northern North Sea) where normal faults are
527 present, in contrast to homoclinal ramp-like relief characterising the distal margins of foreland basins; in

528 the latter, lithology and structural; style changes are more gradual, occurring over several tens of kilometres.
529 We argue that the lack of salt structures on intra-basin structural highs does not simply reflect post-
530 depositional uplift and erosion, but may instead indicate areas where salt tectonics never occurred due to
531 the evaporite-bearing sequence lacking low-viscosity, mobile lithologies (e.g. halite, potash salt). Salt basin
532 morphology is thus a key control on lithology distribution in salt giants, and the resulting spatial variations
533 in the mechanical-stratigraphic of the pre-rift template may directly govern structural styles during
534 subsequent phases of crustal extension (e.g. Jackson & Lewis, 2016).

535

536 **CONCLUSIONS**

537

538 We used 2D seismic reflection and well data to map basin-scale variations in the thickness and composition
539 of the evaporite-dominated Zechstein Supergroup (Lopingian) in the Norwegian sector of the northern
540 North Sea. We showed that the Zechstein Supergroup is dominated by halite, anhydrite and carbonate, with
541 relatively minor amounts of claystone, sandstone and potassium salts (carnallite). Based on the proportion
542 of halite, we identified and mapped four intrasalt *depositional zones* (DZs; *sensu* Clark et al., 1998),
543 showing that the Zechstein Supergroup is relatively thin (<200 m), halite-poor (i.e. DZ1 and 2), and
544 relatively enriched in anhydrite and non-evaporitic lithologies (claystone, carbonate and siltstone-
545 sandstone) at the basin margins and on normal-fault bound, intra-basin structural highs. In contrast, the
546 Zechstein Supergroup is relatively thick (>200 m) and halite-rich (i.e. DZ3 and 4) in the relatively deep,
547 normal fault-bound basins; in these locations, anhydrite and claystone are rare, forming part of caprock
548 sequences developed at the crests of salt diapirs and pillows. Transitions between these domains are either
549 abrupt, occurring across large, basement-involved normal faults, or more gradational, occurring along
550 largely unfaulted, gently-dipping ramps. Similar relationships between evaporite thickness and
551 composition, and structural position (i.e. structural high vs. basin) are observed in the UK sector of the
552 northern North Sea and in other ancient salt giants. It is presently unclear if the variability observed in the
553 northern North Sea reflects variations in syn-depositional relief related to flooding of an underfilled presalt
554 (Early Permian) rift or syn-depositional (Lopingian) rift-related faulting. Irrespective of the underlying
555 controls, variations in salt composition and thickness clearly influenced the Middle Jurassic-to-Early
556 Cretaceous rift structural style, with diapirism characterising hangingwall basins where autochthonous salt
557 was thick and halite-rich, and salt-detached normal faulting occurring on the basin margins and on intra-
558 basin structural highs where the salt was too thin and/or halite-poor to undergo diapirism. Furthermore, the
559 thickness and composition of the Zechstein Supergroup impact the degree of sub- and supra-salt kinematic
560 coupling, with these structural levels being coupled where the unit is thin and halite-poor, and poorly

561 coupled where it is thick and halite-rich. This variability is currently not captured by existing tectono-
562 stratigraphic models largely based on observations from salt-free rifts. We suggest mapping of suprasalt
563 structural styles (e.g. diapirs, salt-detached normal faults), in addition to subsalt structural highs and low
564 (e.g. halite-rich basins, halite-poor structural highs), may provide insights into salt composition and
565 thickness in areas where boreholes are lacking or seismic imaging is poor.

566

567 **ACKNOWLEDGMENTS**

568 This research presented in this paper formed part of the Statoil-funded Salt-Influenced Rift Basins (SIRB)
569 project, which was based at Imperial College, the University of Manchester and the University of Bergen.
570 We would like to acknowledge the technical input of numerous people based in the Norwegian North Sea
571 South Licenses Team (Stavanger) and in the Research Centre (Bergen). We would also like to acknowledge
572 Schlumberger for providing Petrel to all three institutes. Robin Warner, Aruna Mannie and Matthew Lewis
573 are also thanked for their contribution to elements of the work presented here.

574

575 **REFERENCES**

576

577 BAARS, D.L. & STEVENSON, G.M. (1981) Tectonic evolution of the Paradox basin, Utah and Colorado.
578 In: *Geology of the Paradox Basin* (Ed. by D.L. Wiegand), pp. 23-31. Association of Geologists, Rocky
579 Mount.

580

581 BAARS, D.L. (1983) *The Colorado Plateau, a geologic history*. University of New Mexico Press.

582

583 BACHMANN, G.H., GELUK, M.C., WARRINGTON, G., BECKER-ROMAN, A., BEUTLER, G.,
584 HAGDORN, H., HOUNSLOW, M.W., NITSCH, E., RÖHLING, H.-G., SIMON, T. & SZULC, A.
585 (2010) Triassic. In: Doornenbal, J.C. and Stevenson, A.G. (editors): *Petroleum Geological Atlas of the*
586 *Southern Permian Basin Area*. EAGE Publications b.v. (Houten), 149-173.

587

588 BARBEAU, D.L. (2003) A flexural model for the Paradox Basin: implications for the tectonics of the
589 Ancestral Rocky Mountains. *Basin Research*, **15**, 97-115.

590

591 BARTHOLOMEW, I.D., PETERS, J.M. & POWELL, C.M. (1993) Regional structural evolution of the
592 North Sea: oblique-slip and reactivation of basement lineaments. In: *Petroleum Geology of Northwest*

593 *Europe: Proceedings of the 4th Conference* (Ed. by J.R. Parker), pp. 1109-1122. Geological Society,
594 London.

595

596 BIDDLE, K.T. & RUDOLPH, K.W. (1988) Early tertiary structural inversion in the Stord basin, Norwegian
597 north sea. *Journal of the Geological Society*, **145**, 603-611.

598

599 BISHOP, D.J. (1996) Regional distribution and geometry of salt diapirs and supra-Zechstein Group faults
600 in the western and central North Sea, *Mar. Petrol. Geol.*, **13**, 355-364.

601

602 BRANTHER, S.R.F. (2003) The East Brae field, blocks 16/03a, 16/03b, UK North Sea. In: *United Kingdom*
603 *Oil and Gas Fields, Commemorative Millennium Volume* (Ed. by J. Gluyas & H.M. Hichens),
604 *Geological Society, London, Memoir 20*, 191-197.

605

606 BREHM, J.A. (2003) The North and Beinn fields, block 16/7a, UK North Sea. In: *United Kingdom Oil and*
607 *Gas Fields, Commemorative Millennium Volume* (Ed. by J. Gluyas & H.M. Hichens), *Geological*
608 *Society, London, Memoir 20*, 199-209.

609

610 BROWN, A. (2004) Interpretation of three-dimensional seismic data. AAPG Memoir 42, SEG
611 Investigations in Geophysics, 9.6th edn.

612

613 BURLIGA, S., KOYI, H.A., CHEMIA, Z (2012) Analogue and numerical modelling of salt supply to a
614 diapiric structure rising above an active basement fault. In: *Salt Tectonics, Sediment and Prospectivity*.
615 (Ed. by G.I. Alsop, S.G. Archer, A.J. Hartley, N.T. Grant, R. Hodgkinson), *Geol. Soc. London Spec.*
616 *Publ.*, 363, 395-408.

617

618 CARTWRIGHT, J.A. (1989) The kinematics of inversion in the Danish Central Graben. *Geological*
619 *Society, London, Special Publications*, 44, 153-175.

620

621 CARTWRIGHT, J.A., STEWART, S. & CLARK, J. (2001) Salt dissolution and salt-related deformation
622 of the Forth Approaches Basin, UK North Sea. *Mar. Petrol. Geol.*, **18**, 757-778.

623

624 CARTWRIGHT, J.A., JACKSON, M.P.A, DOOLEY, T., AND HIGGINS, S., 2012, Strain partitioning in
625 gravity-driven shortening of a thick, multilayered evaporite sequence, in Alsop, G.I., et al., eds., *Salt*

626 Tectonics, Sediments and Prospectivity: Geological Society of London Special Publication 363, p. 449–
627 470,
628
629 CHERRY, S.T.J. (1993) The interaction of structure and sedimentary process controlling deposition of the
630 Upper Jurassic Brae formation Conglomerate, block 16/17, North Sea. In: *Petroleum Geology of*
631 *Northwest Europe: Proceedings of the 4th Conference* (Ed. by J.R. Parker), pp. 387-400. Geological
632 Society, London.
633
634 CLARK, J.A., STEWART, S.A. & CARTWRIGHT, J.A. (1998) Evolution of the NW margin of the North
635 Permian Basin, UK North Sea. *J. Geol. Soc. of London*, **155**, 663-676.
636
637 COCKINGS, J.H., KESSLER, L.G. II, MAZZA, T.A., & RILEY, L.A. (1992) Bathonian to mid-Oxfordian
638 sequence stratigraphy of the South Viking Graben, North Sea. In: *Exploration Britain: Insights for the*
639 *Next Decade* (Ed. by R.F.P. Hardman), *Geol. Soc. London Spec. Publ.*, **67**, 65–105.
640
641 COWARD, M.P. (1995) Structural and tectonic setting of the Permo-Triassic basins of Northwest Europe.
642 In: *Permian and Triassic Rifting in Northwest Europe* (Ed. by S.A.R. Boldy), **91**, 7-39.
643
644 COWARD, M.P., DEWEY, J.F., HEMPTON, M. & HOLROYD, J. (2003) Tectonic evolution. In: *The*
645 *Millennium Atlas: Petroleum Geology of the Central and Northern North Sea* (Ed. by D. Evans, C.
646 Graham, A. Armour & P. Bathurst), 17-33. The Geological Society of London, London.
647
648 DAVIES, R., DONNELL, D., BENTHAM, P.N., GIBSON, J.P.C., CURRY, M.R., DUNAY, R.E. &
649 MAYNARD, J.R. (1999) The origina and genesis of major Jurassic unconformities within the triple
650 junction area of the North Sea, UK. In: *Petroleum Geology of Northwest Europe: Proceedings of the*
651 *5th conference* (Ed. by A.J. Fleet & S.A.R. Boldy), pp. 117-131. Geological Society, London.
652
653 DAVISON, I., ALSOP, I. & BIRCH, P. (2000) Geometry and late-stage structural evolution of Central
654 Graben salt diapirs, North Sea. *Mar. Petrol. Geol.*, **17**, 499-522.
655
656 DE FREITAS, R.T.J. (2006) Ciclos Depositionais Evaporiticos Da Bacia De Santos: Uma Analise
657 Cicloestratigrafica a Partir De Dados De 2 Pocos E De Tracos De Sismica., Universidade Federal do
658 Rio Grande do Sul, Brazil.

659
660 DOOLEY, T., MCCLAY, K.R., HEMPTON, M. AND SMIT, D., 2005, January. Salt tectonics above
661 complex basement extensional fault systems: results from analogue modelling. In Geological Society,
662 London, Petroleum Geology Conference series (Vol. 6, No. 1, pp. 1631-1648). Geological Society of
663 London.
664
665 DUFFY, O.B., GAWTHORPE, R.L., DOCHERTY, M. & BROCKLEHURST, S.H. (2013) Mobile
666 evaporite controls on the structural style and evolution of rift basins. *Basin Research*, **25**, 310–330.
667
668 ERRATT, D. (1993) Relationships between basement faulting, salt withdrawal and Late Jurassic rifting,
669 UK Central North Sea. In: *Petroleum Geology of Northwest Europe: Proceedings of the 4th Conference*
670 (Ed. by J. R. Parker), pp. 1211-1219. Geological Society, London.
671
672 ERRATT, D., THOMAS, G.M. & WALL G.R.T. (1999) The evolution of the Central North Sea Rift. In:
673 *Petroleum Geology of Northwest Europe: Proceedings of the 5th conference* (Ed by A.J. Fleet & S.A.R.
674 Boldy), pp. 63-82. Geological Society, London.
675
676 EVANS D., ARMOUR, A., BATHURST, P., GAMMAGE, J., SWALLOW, J., GRAHAM, C. &
677 STEWART, H. (2003) *Millennium Atlas: Petroleum Geology of Central & Northern North Sea*.
678 London, The Geological Society of London, 390p.
679
680 FLETCHER, K.J. (2003a) The Central Brae field, blocks 16/07a, 16/07b, UK North Sea. In: *United*
681 *Kingdom Oil and Gas Fields, Commemorative Millennium Volume* (Ed. by J. Gluyas & H.M. Hichens),
682 **20**, 183-190. Geological Society of London.
683
684 FLETCHER, K.J. (2003b) The South Brae field, blocks 16/07a, 16/07b, UK North Sea. In: *United Kingdom*
685 *Oil and Gas Fields, Commemorative Millennium Volume* (Ed. by J. Gluyas & H.M. Hichens), **20**, 211-
686 221. Geological Society of London.
687
688 FRASER, S.I., ROBINSON, A.M., JOHNSON, H.D., UNDERHILL, J.R., KADOLSKY, D.G.A.,
689 CONNELL, R., JOHANNESSEN, P. & RAVNAS, R. (2003) Upper Jurassic. In: *The Millennium Atlas:*
690 *Petroleum Geology of the Central and Northern North Sea* (Ed. by D. Evans, C. Graham, A. Armour &
691 P. Bathurst), pp. 157-189. The Geological Society of London, London.

692
693 GAMBÔA, L.A.P., MACHADO, M.A.P., SILVEIRA, D.P., DE FREITAS, J.T.R. & DA SILVA, S.R.P.
694 (2008) Evaporitos Estratificados No Atlantico Sul: Interpretacao Sismica E Controle Tectono-
695 Estratigrafico Na Bacia De Santos. In Mohriak, W., Szatmari, P. & Anjos, S.M.C. Sal: Geologia e
696 Tectonica, Exemplos nas Basicas Brasileiras., Beca Edicoes Ltda, Sao Paulo, Brasil, 340-359.
697
698 GLENNIE, K.W., HIGHMAN J., & STEMMERIK, L. (2003) Permian. In: *The Millennium Atlas:*
699 *petroleum geology of the central and northern North Sea* (Ed by D. Evans, C. Graham, A. Armour & P.
700 Bathurst), pp. 91-103. The Geological Society of London, London.
701
702 GOLDSMITH, P.J., HUDSON, G. & VAN VEEN, P. (2003) Triassic. In: *The Millennium Atlas: petroleum*
703 *geology of the central and northern North Sea* (Ed by D. Evans, C. Graham, A. Armour & P. Bathurst),
704 pp. 105-127. The Geological Society of London, London.
705
706 HODGSON, N.A., FARNSWORTH, J. & FRASER, A.J. (1992) Salt-related tectonics, sedimentation and
707 hydrocarbon plays in the Central Graben, North Sea, UKCS. In: *Exploration Britain: Geological*
708 *Insights for the Next Decade.* (Ed. by R.F.P. Hardman), *Geol. Soc. London Spec. Publ.*, **67**, 31–63.
709
710 HSÜ, K.J. (1972) Origin of saline giants: a critical review after the discovery of the Mediterranean
711 evaporite. *Earth-Science Reviews*, **8**, 371-396.
712
713 HUDEC, M.R. & JACKSON, M.P.A. (2007) Terra infirma: Understanding salt tectonics. *Earth- Science*
714 *Reviews*, **82**, 1-28.
715
716 JACKSON, M.P.A., VENDEVILLE, B.C. & ELA-SCHULTZ, D.D. (1994) Structural dynamics of salt
717 systems. *Annual Review of Earth and Planetary Sciences*, **22**, 93-117.
718
719 JACKSON, M.P.A. & VENDEVILLE, B.C. (1994) Regional extension as a geologic trigger for diapirism.
720 *Geological Society of America Bulletin*, **106**, 57-73.
721
722 JACKSON, M.P.A. & HUDEC, M.R., 2017. Salt tectonics: Principles and practice. Cambridge University
723 Press.
724

725 JACKSON, C.A-L. & LARSEN, E. (2008) Temporal constraints on basin inversion provided by 3D seismic
726 and well data: a case study from the SVG. *Basin Ressearch*, **20**, 397-417.
727

728 JACKSON, C.A-L. & E. LARSEN (2009) Temporal and spatial development of a gravity-driven normal
729 fault array: Middle–Upper Jurassic, South Viking Graben, northern North Sea. *J. Struct. Geol.*, **31**, 388
730 – 402.
731

732 JACKSON, C.A-L., KANE, K.E. & LARSEN, E (2010) Structural evolution of minibasins on the Utsira
733 High, northern North Sea; implications for Jurassic sediment dispersal and reservoir distribution. *Pet.*
734 *Geosci.*, **16**, 105-120.
735

736 JACKSON, C.A-L. & LEWIS, M.M (2013) Physiography of the NE margin of the Permian Salt Basin:
737 new insights from 3D seismic reflection data. *Journal of the Geological Society*, **170**, 857-860.
738

739 JACKSON, C.A-L. & LEWIS M.M, (2016) Structural style and evolution of a salt-influenced rift basin
740 margin: the impact of variations in salt composition and the role of polyphase extension. *Basin Research*,
741 **28**, 81-102.
742

743 JACKSON, C.A.L., RODRIGUEZ, C.R., ROTEVATN, A., AND BELL, R.E., 2014a, Geological and
744 geophysical expression of a primary salt weld: An example from the Santos Basin, Brazil: Interpretation,
745 v. 2, p. SM77–SM89.
746

747 JACKSON, C.A-L. & STEWART, S.A. (2017) Composition, Tectonics, and Hydrocarbon Significance of
748 Zechstein Supergroup Salt on the United Kingdom and Norwegian Continental Shelves: A Review. In
749 *Permo-Triassic Salt Provinces of Europe, North Africa and the Atlantic Margins* (175-201).
750

751 KANE K.E., C.A-L. JACKSON & E. LARSEN (2010) Normal fault growth and fault-related folding in a
752 salt-influenced rift basin: South Viking Graben, Offshore Norway. *J. Struct. Geol.*, **32** (4), 490-506.
753

754 KNOTT, S.D., BURCHELL, M.T., JOLLEY, E.J. & FRASER, A.J. (1993) Mesozoic to Cenozoic plate
755 reconstructions of the North Atlantic and hydrocarbon plays of the Atlantic margins. In: *Petroleum*
756 *Geology of Northwest Europe: Proceedings of the 4th Conference* (Ed. by J.R. Parker), pp. 953-974.
757 Geological Society, London.

758
759 KNOTT, S.D. (2001) Gravity-driven crustal shortening in failed rifts. *J. Geol. Soc.*, **158**, 193-196.
760
761 KOYI, H., JENYON, M.K. & PETERSON, K. (1993) The effect of basement faulting on diapirism. *J.*
762 *Petrol. Geol.*, **16**, 285-312.
763
764 KRZYWIEC, P. (2012) Mesozoic and Cenozoic evolution of salt structures within the Polish Basin: An
765 overview. In: Salt Tectonics, Sediment and Prospectivity. (Ed. by G.I. Alsop, S.G. Archer, A.J. Hartley,
766 N.T. Grant, R. Hodgkinson), Geol. Soc. London Spec. Publ., **363**, 381–394.
767
768 KUPFER, D.H., 1968, Relationship of internal to external structure of salt domes, in Braunstein, J., ed.,
769 Diapirism and Diapirs: American Association of Petroleum Geologists Memoir 8, p. 79–80.
770
771 LEWIS, M.M., JACKSON, C.A-L. & GAWTHORPE, R.L. (2013) Salt-influenced normal fault growth
772 and forced folding: The Stavanger Fault System, North Sea. *Journal of Structural Geology*, **54**, 156-173.
773
774 LYNGSIE, S.B., THYBO, H. & RASMUSSEN, T.M. (2006) Regional geological and tectonic structures
775 of the North Sea area from potential field modelling. *Tectonophysics*, **413**, 147-170.
776
777 MARSH, N., IMBER, J., HOLDSWORTH, R.E., BROCKBANK, P. & RINGROSE, P. (2009) The
778 structural evolution of the Halten Terrace, offshore Mid-Norway: extensional fault growth and strain
779 localisation in a multi-layer brittle-ductile system. *Basin Res.*, **22**, 195-214.
780
781 MATTHEWS, W.J., HAMPSON, G.J., TRUDGILL, B.D. & UNDERHILL, J.R. (2007) Controls on fluvio-
782 lacustrine reservoir distribution and architecture in passive salt diapir provinces: insights from outcrop
783 analogs. *Am. Assoc. Petrol. Geol. Bull.*, **91**, 1367-1403.
784
785 MCKIE, T. (2017) Paleogeographic Evolution of Latest Permian and Triassic Salt Basins in Northwest
786 Europe. In *Permo-Triassic Salt Provinces of Europe, North Africa and the Atlantic Margins*, 159-173.
787 Elsevier.
788

789 MILTON, N.J. (1993) Evolving depositional geometries in the North Sea Jurassic rift. In: *Petroleum*
790 *Geology of Northwest Europe: Proceedings of the 4th Conference* (Ed by J.R. Parker), pp. 425-442.
791 Geological Society London.
792

793 MOREIRA, J.L.P., MADEIRA, C., GIL, J.A. & MACHADO, M.A.P. (2007) Bacia De Santos. Bulletin
794 Geociencias Petrobras, 15, 531-549.
795

796 PEGRUM, R.M. & LJONES, T.E. (1984) 15/9 Gamma gas field offshore Norway, new trap type for the
797 North Sea basin with regional structural implications. *AAPG Bull.*, **68**, 874-902.
798

799 PENGE, J., TAYLOR, B., HUCKERBY, J.A. & MUNNS, J.W. (1993) Extension and salt tectonics in the
800 East Central Graben. In: *Petroleum Geology of Northwest Europe: Proceedings of the 4th Conference*
801 (Ed. by J.R. Parker), pp. 1197-1210. Geological Society of London.
802

803 RICHARDSON, N.J., UNDERHILL, J.R. & LEWIS, G. (2005) The role of evaporite mobility in modifying
804 subsidence patterns during normal fault growth and linkage, Halten Terrace, Mid-Norway. *Basin Res.*,
805 **17**, 203–223.
806

807 ROBERTS, A.M., YIELDING, G., KUSZNIR, N.J., WALKER, I.M. & DORN-LOPEZ, D. (1995)
808 Quantitative analysis of Triassic extension in the Northern Viking Graben. *J. Geol. Soc.*, **152**, 15-26.
809

810 ROWAN, M.G. & WEIMER, P. (1998) Salt-Sediment interaction, Northern Green Canyon and Edwing
811 Bank (Offshore Louisiana), Northern Gulf of Mexico. *AAPG Bull.*, **82**, 1055-1082.
812

813 Rowan, M.G. (2014) Passive-margin salt basins: hyperextension, evaporite deposition, and salt tectonics.
814 *Basin Research*, **26**, 154-182.
815

816 SCHLUMBERGER (1985) Log interpretation charts, Schlumberger Publication.
817

818 SCHLUMBERGER (1989a) Log interpretation, principles and applications, Schlumberger Educational
819 Services.
820

821 SCHLUMBERGER (2009) Log Interpretation Charts. 2009 Edition, Schlumberger Publication.

822
823 SHELLEY, D.C. & LAWTON, T.F. (2005) Sequence stratigraphy of tidally-influenced deposits in a salt-
824 withdrawal minibasin: Upper sandstone member of the Potrerillos Formation (Paleocene), La Popa basin
825 Mexico. *Am. Assoc. Petrol. Geol. Bull.*, **89**, 1157-1179.
826
827 SMITH, R.I., HODGSON, N., & FULTON, M. (1993) Salt control on Triassic reservoir distribution, UKCS
828 Central North Sea. In: *Petroleum Geology of Northwest Europe: Proceedings of the 4th Conference* (Ed
829 by J.R. Parker), pp. 547-557. Geological Society London.
830
831 SOTO, J.I., FLINCH, J.F. & TARI, G. (2017) Permo-Triassic Basins and Tectonics in Europe, North Africa
832 and the Atlantic Margins: A Synthesis. In *Permo-Triassic Salt Provinces of Europe, North Africa and*
833 *the Atlantic Margins*, 3-41. Elsevier.
834
835 STEWART, S.A. (2018) Hormuz salt distribution and influence on structural style in NE Saudi Arabia.
836 *Petroleum Geoscience*, **24**, 143-158.
837
838 STEWART, S.A. & COWARD, M.P. (1995) Synthesis of salt tectonics in the southern North Sea, UK.
839 *Mar. Petrol. Geol.*, **12**, 457-475.
840
841 STEWART, S.A., HARVEY, M.J., OTTO, S.C. & WESTON, P.J. (1996) Influence of salt on fault
842 geometry: examples from the UK salt basins. In: *Salt Tectonics* (Ed. by Alsop G.I., Blundell D.J.,
843 Davison I.) *Geol. Soc. Spec. Publ.*, 100, 175–202.
844
845 STEWART, S.A. & CLARK, J.A. (1999) Impact of salt on the structure of the Central North Sea
846 hydrocarbon fairways. In: *Petroleum Geology of Northwest Europe: Proceedings of the 5th Conference*
847 (Ed by A. J. Fleet & S.A.R. Boldy), pp. 179-200. Geological Society London.
848
849 STEWART, S.A. (2007) Salt tectonics in the North Sea Basin: a structural style template for seismic
850 interpreters. In: *Deformation of the Continental Crust: The Legacy of Mike Coward* (Ed. by A.C. Ries,
851 R.W.H. Butler & R.H. Graham). *Geol. Soc. London Spec. Publ.*, **272**, 361-396.
852
853 SØRENSEN, S., MORIZOT, H. & SKOTTHEIM, S. (1992) A tectonostratigraphic analysis of the
854 southeast Norwegian North Sea Basin. In: *Structural and Tectonic Modelling and its Application to*

855 *Petroleum Geology: Proceedings of the Norwegian Petroleum Society Workshop* (Ed. by R.M. Larsen,
856 H. Brekke, B.T. Larsen & E. Talleraas). Amsterdam, Elsevier, 19-42.
857
858 TAYLOR, J.C.M. (1990) Upper Permian-Zechstein. In: *Introduction to the Petroleum Geology of the North*
859 *Sea* (Ed. by K.W. Glennie, 3rd Edition). Blackwell Scientific Publications, 153-190.
860
861 THOMAS, D.W. & COWARD, M.P. (1996) Mesozoic regional tectonics and South Viking Graben
862 formation; evidence for localized thin-skinned detachments during rift development and inversion. *Mar.*
863 *Petrol. Geol.*, **13**, 149-177.
864
865 TRUDGILL, B., BANBURY, N. & UNDERHILL, J. (2004) Salt evolution as a control on structural and
866 stratigraphic systems: northern Paradox foreland basin, SE Utah, USA. In: *Salt Sediment Interactions*
867 *and hydrocarbon Prospectivity: Proceedings of 24th Annual Gulf Coast Section SEPM Foundation Bob*
868 *F. Perkins research conference* (Ed. by P.J. Post, D.L. Olson, K.T. Lyons, S.L. Palmes, P.F. Harrison
869 & N.C. Rosen), pp 669-700.
870
871 TRUDGILL, B.D. (2011) Evolution of salt structures in the northern Paradox Basin: controls on evaporite
872 deposition, salt wall growth and supra-salt stratigraphic architecture. *Basin Res.*, **23**, 208–238.
873 TUCKER, M.E. (1991) Sequence stratigraphy of carbonate-evaporite basins: models and application to the
874 Upper Permian (Zechstein) of northeast England and adjoining North Sea. *Journal of the Geological*
875 *Society*, **148**, pp.1019-1036.
876
877 TVEDT, A.B.M, ROTEVATN, A., JACKSON, C.A-L., FOSSEN, H. & GAWTHORPE, R.L. (2013)
878 Growth of normal faults in multilayer sequences: a 3D seismic case study from the Egersund Basin,
879 Norwegian North Sea. *Journal of Structural Geology*, **55**, 1-20.
880
881 UNDERHILL, J.R. & PARTINGTON, M.A. (1993) Jurassic thermal doming and deflation in the North
882 Sea: implications of the sequence stratigraphic evidence. In: *Petroleum Geology of Northwest Europe:*
883 *Proceedings of the 4th Conference* (Ed. by J.R. Parker), pp. 337-345. Geological Society, London.
884
885 VENDEVILLE, B.C. & JACKSON, M.P.A. (1992) The rise of diapirs during thin-skinned extension.
886 *Marine and Petroleum Geology*, **9**, 331-354.
887

- 888 WARREN, J.K. (2010) Evaporites through time: Tectonic, climatic and eustatic controls in marine and
889 nonmarine deposits. *Earth-Science Reviews*, **98**, 217-268.
- 890
- 891 WARREN, J.K. (2016) Evaporites: A geological compendium. Springer.
- 892
- 893 WILLIAMS, G.D. (1993) Structural models for the evolution of the North Sea area. In: *Petroleum Geology*
894 *of Northwest Europe: Proceedings of the 4th conference* (Ed. by J.R. Parker), pp. 1083-1093. Geological
895 Society of London.
- 896
- 897 WILSON, P., ELLIOTT, G.M., GAWTHORPE, R.L., JACKSON, C.A.-L., MICHELSEN, L. & SHARP,
898 I.R. (2013) Geometry and segmentation of an evaporite-detached normal fault array: the southern
899 Bremstein Fault Complex, offshore mid-Norway. *J. Struct. Geol.*, **51**, 74–91.
- 900
- 901 WITHJACK, M.O. & CALLAWAY, S. (2000) Active normal faulting beneath a salt layer: an experimental
902 study of deformation patterns in the cover sequence. *AAPG Bull.*, **84**, 627-651.
- 903
- 904 ZANELLA, E. & COWARD, M.P. (2003) Structural framework. In: *The Millenium Atlas: petroleum*
905 *geology of the central and northern North Sea* (Ed. by D. Evans, C. Graham, A. Armour & P. Bathurst),
906 pp. 45-59. The Geological Society of London.
- 907
- 908 ZIEGLER, P.A. (1990) Tectonic and paleogeographic development of the North Sea rift system. In:
909 *Tectonic Evolution of the North Sea Rifts* (Ed. by D. Blundell & A.D. Gibbs), pp. 1-36. Clarendon Press,
910 Oxford.
- 911
- 912 ZIEGLER, P.A. (1992) Geodynamic of rifting and implications for hydrocarbon habitat, *Tectonophysics*,
913 **215**, 221-253.
- 914

915 **FIGURE CAPTIONS**

916

917 **Fig. 1.** Simplified structural basemap of the study area indicating the position of major basement-involved
918 normal faults, sub-basins and intra-basin structural highs. FGS=Fladen Ground Spur; SVG=South Viking
919 Graben; WGG=Witch Ground Graben; SB=Sleipner Basin; ST=Sleipner Terrace; UH=Utsira High;
920 LD=Ling Depression; SH=Sele High; AG=Åsta Graben; EB=Egersund Basin; SP=Stavanger Platform;

921 LN=Lista Nose; N-DB=Norwegian-Danish Basin. The seismic and borehole dataset used in this study is
922 shown. The regional geographical setting of the North (NPB) and South (SPB) Permian basins is shown in
923 the inset map.

924

925 **Fig. 2.** Composite stratigraphic column for the study area. The regional tectono-stratigraphic significance
926 of the various stratigraphic units is indicated (modified from Jackson and Larsen, 2009).

927

928 **Fig. 3.** (a) Map showing the principal lithologies in the Zechstein Supergroup (Upper Permian) along the
929 northwestern margin of the NPB (UK sector of the Central Graben) and their relationship to the main
930 basement-involved structural elements (modified from Stewart, 2007). Four depositional zones (DZs) are
931 depicted (1-4), which are differentiated based on their proportion of halite (Clark *et al.*, 1998). Areas of
932 syn-depositional (i.e. Lopingian) and immediately post-depositional (i.e. Triassic) salt flow are indicated.
933 The red box represents the area considered in our study. (b) Schematic section showing the idealized lateral
934 lithology variability observed between the centre and the margin of an evaporite basin (based on the west
935 margin of the Southern Permian Basin; see Taylor, 1990). Four DZs corresponding to those shown in (a)
936 and which are defined by varying proportions of halite, are recognised.

937

938 **Fig. 4.** Density (RHOB) vs. sonic (DT) cross-plot illustrating the petrophysical expression of the evaporite
939 and non-evaporite lithologies recovered in cuttings from the Zechstein Supergroup. For the location of
940 boreholes see Fig. 1. Note the strong (anhydrite) to very strong (halite) differentiate between evaporite and
941 non-evaporite lithologies. ‘Ideal’ values reported by Schlumberger (2009) for RHOB and DT are indicated
942 by a black dot with a red outline (halite) and a black dot with a blue outline (anhydrite). Note that these
943 ideal values are for pure mineral species (i.e. they do not account for impure rock types that contain a mix
944 of minerals with different physical characteristics).

945

946 **Fig. 5.** (a) Sonic (DT) vs. gamma-ray (GR) and (b) density (RHOB) vs. gamma-ray (GR) cross-plot
947 illustrating the petrophysical expression of claystone and carbonate recovered in cutting from the Zechstein
948 Supergroup. For the location of boreholes see Fig. 1. Note the strong overlap between these two non-
949 evaporite lithologies.

950

951 **Fig. 6.** Regional Zechstein Supergroup isochron based on mapping of 2D seismic profiles shown in Fig. 1.
952 The present depositional/erosional limit of the Zechstein Supergroup is shown, in addition to the locations
953 of major basement-involved normal faults and key boreholes. Due to gridding artefacts (i.e. spatial aliasing)

954 resulting from gridding of relatively widely spaced (>5 km) 2D seismic profiles, the detailed geometry of
955 individual salt structures and their flanking depocentres (minibasins) is poorly constrained; i.e. structures
956 appearing as isolated, sub-circular stocks might in fact form part of much more continuous, elongate walls.
957 See the caption for Fig. 1 for the abbreviations for key structural elements. For clarity, only selected wells
958 are shown; see Fig. 1 for the spatial of all wells, and Figs 7-10 and 14 for well data.

959

960 **Fig. 7.** Stratigraphic panel (a) and corresponding interpreted seismic profile (b) across the South Viking
961 Graben, Utsira High, Sleipner Terrace and Ling Depression. The stratigraphic panel illustrates the
962 lithological variability between basin centre (i.e. South Viking Graben and Ling Depression) and basin
963 margin (i.e. Utsira High, Sleipner Terrace) locations. The stratigraphic panel is flattened on the top of the
964 Zechstein Supergroup and the lithologies defined in the panel are based on cuttings data. The seismic profile
965 illustrates the structural setting of the wells and their relationships to salt structures. The location of the
966 profile is shown in Fig. 1. GBFZ=Graben Boundary Fault Zone.

967

968 **Fig. 8.** Stratigraphic panel (a) and corresponding interpreted seismic profile (b) across the eastern margin
969 of the South Viking Graben. The stratigraphic panel illustrates the lithological variability observed along
970 the basin margin. The stratigraphic panel is flattened on the top of the Zechstein Supergroup and the
971 lithologies defined in the panel are based on electrofacies characterisation (see Fig. 4 and text for further
972 details). The seismic profile illustrates the structural setting of the wells and their relationships to salt
973 structures. The location of the profile is shown in Fig. 1.

974

975 **Fig. 9.** Stratigraphic panel (a) and corresponding interpreted seismic profile (b) across the Sleipner Terrace
976 and Ling Depression. The stratigraphic panel illustrates the lithological variability between basin centre
977 (i.e. western part of the Ling Depression; 16/8-2) and basin margin (i.e. Sleipner Terrace and eastern part
978 of the Ling Depression; 16/9-1) locations. The stratigraphic panel is flattened on the top of the Zechstein
979 Supergroup and the lithologies defined in the panel are based on cuttings data. The seismic profile illustrates
980 the structural setting of the wells and their relationships to salt structures. The location of the profile is
981 shown in Fig. 1.

982

983 **Fig. 10.** Stratigraphic panel (a) and corresponding interpreted seismic profile (b) across the Ling
984 Depression, Sele High and Åsta Graben. The stratigraphic panel illustrates the lithological variability
985 observed between the basin centre (i.e. Ling and Åsta Graben) and an intra-basin structural high (i.e. Sele
986 High). The stratigraphic panel is flattened on the top of the Zechstein Supergroup and the lithologies defined

987 in the panel are based on electrofacies characterisation (see Fig. 4 and text for further details). The seismic
988 profile illustrates the structural setting of the wells and their relationships to salt structures. The location of
989 the profile is shown in Fig. 1.

990

991 **Fig. 11.** Seismic (a) and geoseismic (b) sections across the eastern margin of the Ling Depression and the
992 western margin of the Sele High; in this position, the boundary between the two structural domains is not
993 fault controlled, and is instead defined by a broadly W- to SW-dipping ramp. This profile covers an area
994 where the Zechstein Supergroup is thought to be relatively halite rich (DZ3 of Clark et al., 1998). The
995 location of the profile is shown in Fig. 1.

996

997 **Fig. 12.** Seismic (a) and geoseismic (b) sections across the eastern margin of the Ling Depression and the
998 western margin of the Sele High; in this position, the boundary between the two structural domains is
999 defined by a relatively large-displacement (600 ms TWT), basement-involved normal fault (F1) (cf. Fig.
1000 11). This profile covers an area where the Zechstein Supergroup is thought to pass from being relatively
1001 halite-rich in a deep basin setting (i.e. the Ling Depression; DZ3 of Clark et al., 1998), to being relatively
1002 halite-poor on the basin margin (i.e. the Sele High). Note that the development of thin-skinned, salt-
1003 detached normal faults on the Sele High suggests some halite is present, thus this area may represent DZ2
1004 of Clark et al. (1998), rather than DZ1. The location of the profile is shown in Fig. 1.

1005

1006 **Fig. 13.** Seismic (a) and geoseismic (b) sections across the eastern margin of the Ling Depression, the
1007 southern Sele High, and the western Egersund Basin; in this position, the eastern and western boundaries
1008 of the Sele High are defined by relatively large-displacement (300-1500 ms TWT), basement-involved
1009 normal faults (F1 and F3). This profile covers an area where the Zechstein Supergroup is thought to pass
1010 from being relatively halite-rich in deep basin settings (i.e. the Ling Depression and Egersund Basin; DZ3-
1011 4 of Clark et al., 1998), to being relatively halite-poor on the basin margin (i.e. the Sele High). Note that
1012 the development of relatively small diapirs and shallow minibasins on the Sele High suggests some halite
1013 is present, thus this area may represent DZ2 of Clark et al. (1998), rather than DZ1. The location of the
1014 profile is shown in Fig. 1.

1015

1016 **Fig. 14.** Stratigraphic panel (a) and corresponding interpreted seismic profile (b) across the eastern part of
1017 the Egersund Basin and the Lista Nose. The stratigraphic panel illustrates the lithological variability
1018 observed near the basin margin. The stratigraphic panel is flattened on the top of the Zechstein Supergroup
1019 and the lithologies defined in the panel are based on electrofacies characterisation (see Fig. 4 and text for

1020 further details). The seismic profile illustrates the structural setting of the wells and their relationships to
1021 salt structures. The location of the profile is shown in Fig. 1. Note that 10/7-1, which appears to penetrate
1022 the lower flank of a diapir, is projected into the section and actually penetrates the immediate footwall of a
1023 basin-bounding fault (see Fig. 15).

1024
1025 **Fig. 15.** Regional map showing the basin-scale distribution of DZs (*sensu* Clark et al., 1998), a proxy for
1026 bulk lithology, in the Zechstein Supergroup (ZSG). In the UK sector, the map is based on data published
1027 by Clark et al. (1998), Glennie et al. (2003), Stewart (2007), and Jackson et al. (2010); data presented in
1028 this study is used to constrain the map in the Norwegian sector. Note that boundaries between domains,
1029 especially within the deep basin (e.g. Egersund Basin, South Viking Graben, Ling Depression) and flanking
1030 ramps are uncertain and undoubtedly gradational; these boundaries are thus shown as dashed rather than
1031 solid lines. Where domain boundaries are fault-controlled, they are likely more abrupt. Because of post-
1032 depositional salt flow, in particular from the halite-rich hangingwalls onto the adjacent fault-bound
1033 footwalls, originally halite-poor areas (DZ1 and 2) may now be characterised by variable thickness salt and
1034 salt diapirs (cf. areas of variable thickness salt and diapirism in Fig. 6).

1035
1036 **Fig. 16.** Four end-member models that may account for the thickness and lithology variations observed in
1037 the Zechstein Supergroup (see also Jackson and Lewis, 2013). (A) Model 1 – thickness and lithology
1038 variations driven by post-depositional tectonics (e.g. normal faulting and regional thermal uplift) results in
1039 halite dissolution and the relative enrichment in non-halite lithologies at the basin margins and on intra-
1040 basin structural highs. Thicker, more halite-rich succession preserved in fault hangingwalls. (B) Model 2 –
1041 thickness and lithology variations driven by post-depositional flow of a heterogeneous Zechstein
1042 Supergroup (i.e. anhydrite-dominated basin margin, halite-dominated basin centre), with flow being
1043 strongly partitioned (i.e. mobile halite preferentially expelled from the basin margin into flanking salt
1044 structures, resulting in local enrichment of non-halite lithologies in areas where Zechstein Supergroup is
1045 thin). (C) Models 3 and 4 – thickness and lithology variations driven by pre- (Model 3) and/or syn- (Model
1046 4) depositional tectonics (e.g. normal faulting and regional thermal uplift). Halite deposition in high
1047 accommodation areas (e.g. basin centre) during sea-level lowstand (see t3) and carbonate/anhydrite
1048 deposition in low accommodation areas (e.g. basin margin) during sea-level highstand (see t4) (cf. Tucker,
1049 1991). In Model 4, variations in the thickness and lithology of the Zechstein Supergroup were simply
1050 augmented by syn-depositional faulting. T1-3=sea-level.

1051

1052 **Table 1.** Summary of the boreholes used in this study. GR=gamma ray; DT=sonic velocity;
1053 RHOB=density. See text for full discussion.

1054

1055 **Table 2.** Petrophysical characteristics of evaporite and non-evaporite lithologies encountered in the
1056 Zechstein Supergroup; this is based on well cuttings, and is partly constrained by values reported by
1057 Schlumberger (2009) and Rider and Kennedy (2011) (values in brackets). Note that published values are
1058 for pure mineral species (i.e. they do not account for impure rock types that contain a mix of minerals with
1059 different physical characteristics).

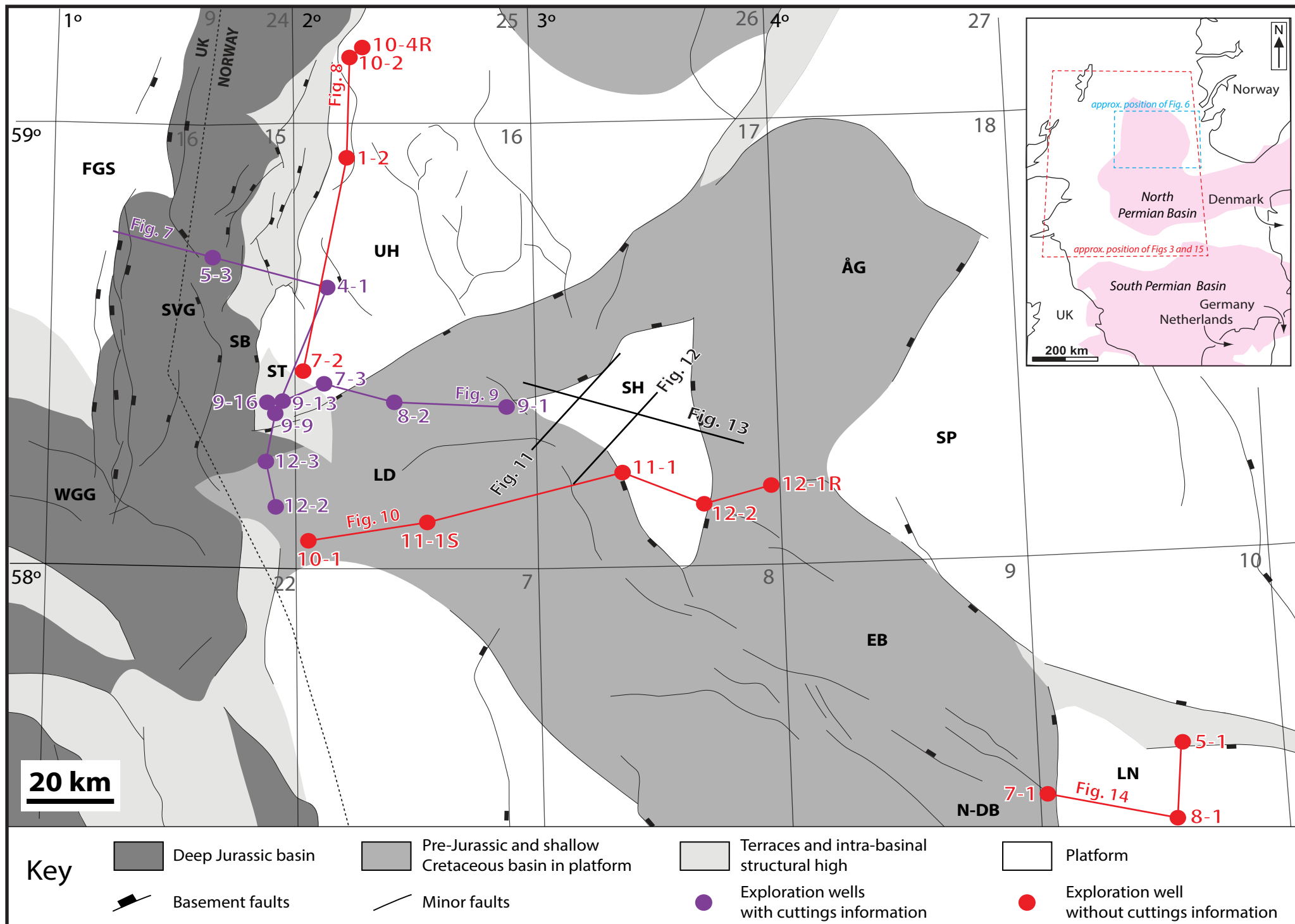


Figure 1

System		SOUTH VIKING GRABEN, UTSIRA HIGH, LING DEPRESSION			EGERSUND BASIN, SELE HIGH			seismic horizons		
		Group	Formation	Tectono-stratigraphic significance	Group	Formation	Tectono-stratigraphic significance			
Cretaceous	Upr.	Chalk	Tor	post-rift	Shetland	Tor	post-rift	top Shetland/ Chalk Gp.		
			Hod			Hod				
			Blodøks							
	Lwr.	Cromer Knoll	Rødby		syn-rift	Cromer Knoll	Rødby		syn-rift	top Viking/ Boknfjord Gp.
			Sola				Sola			
			Åsgard				Åsgard			
Upr.	Viking	Draupne	syn-rift	Boknfjord		Flekkiefjord	syn-rift	top Hegre Gp.		
		Heather				Sauda				
Mid.	Vestland	Hugin				minibasin fill/ rafted blocks				
		Sleipner		Sandnes						
				Bryne						
Triassic		Hegre		Skagerrak	Hegre				Skagerrak	minibasin fill/ rafted blocks
			Smith Bank	Smith Bank						
Permian	Lopingian	Zechstein	pre-rift	Zechstein	pre-rift		evaporite-rich source of salt-tectonic structures/ intrastratal detachment	top Rotliegend Gp.		
	Cisuralian-Guadalupian	Rotliegend	Auk	Rotliegendes	Auk	Basement				

Figure 2

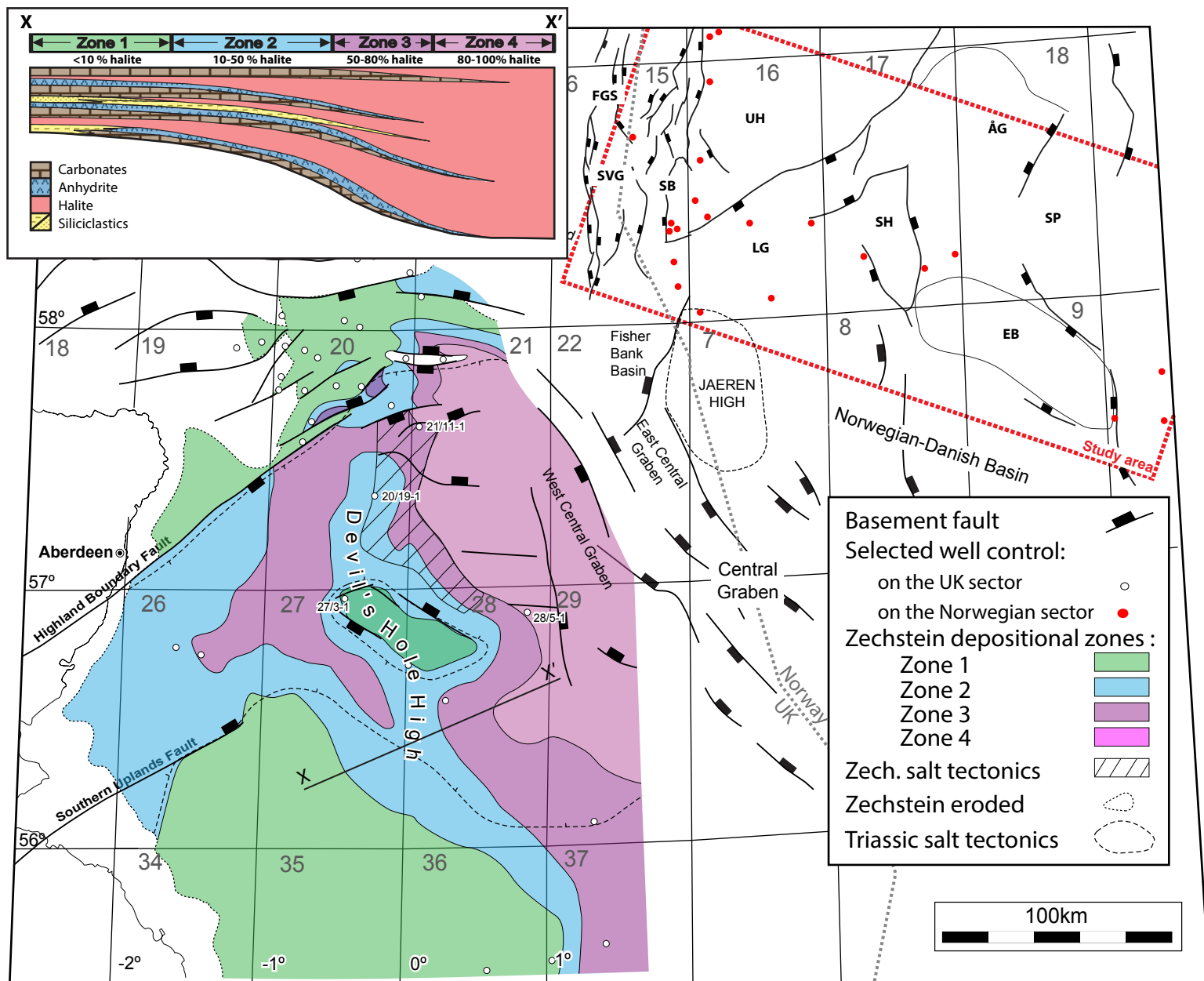


Figure 3

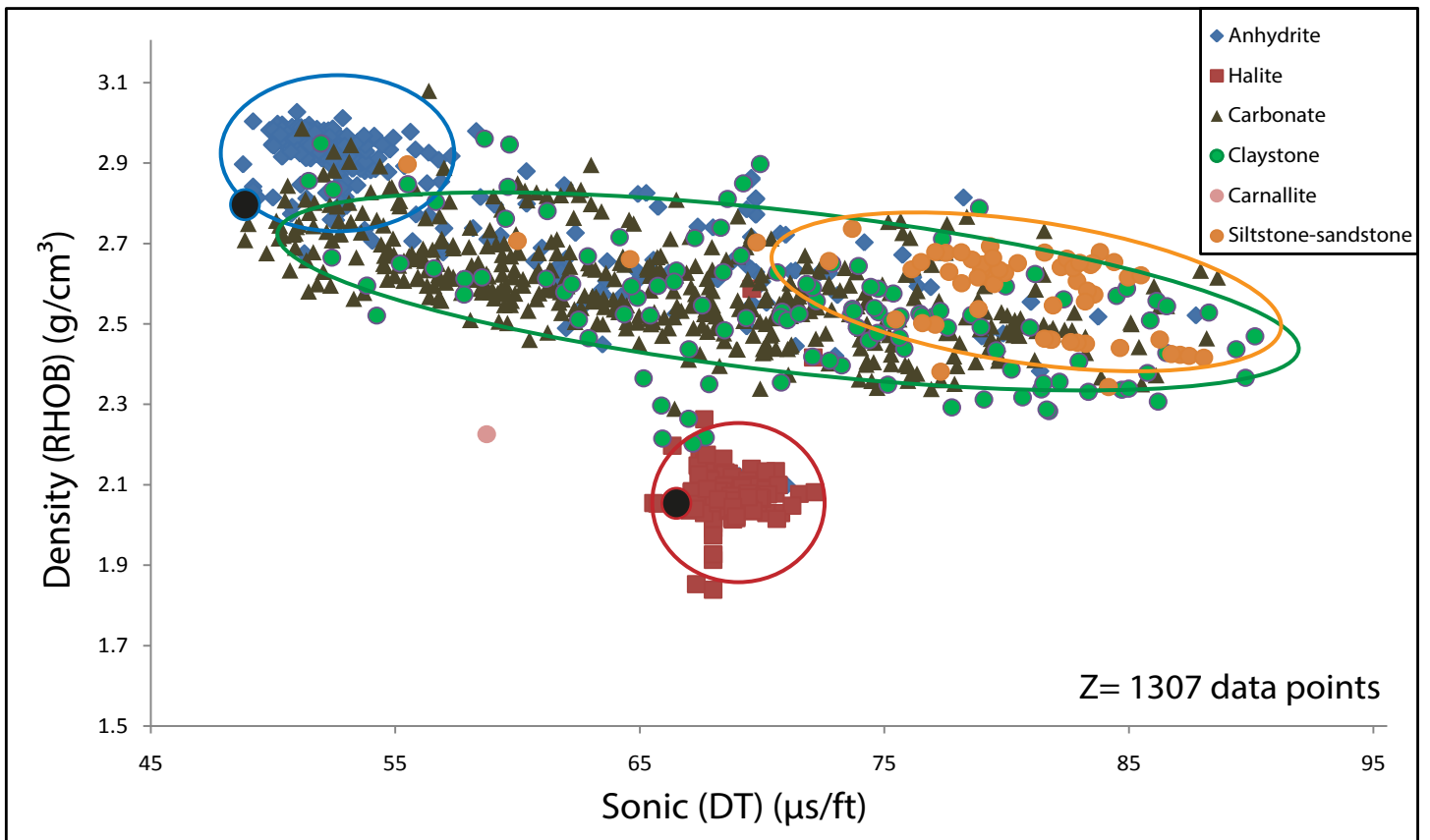


Figure 4

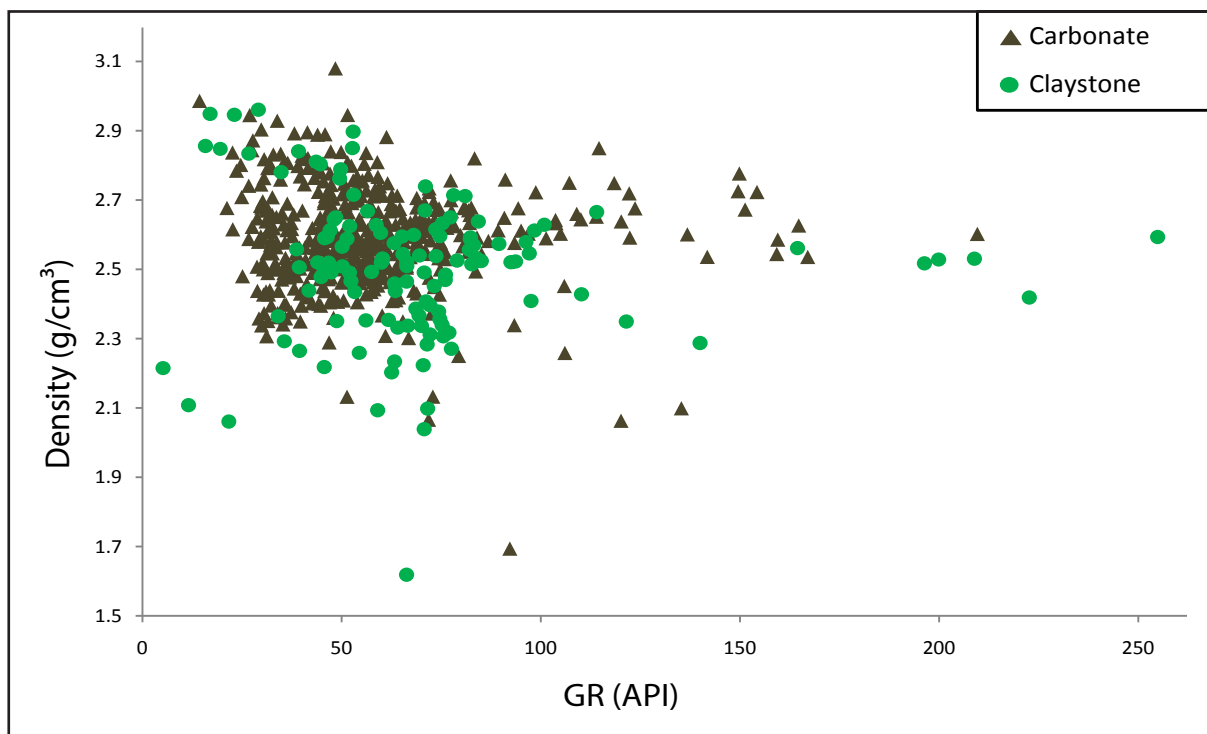
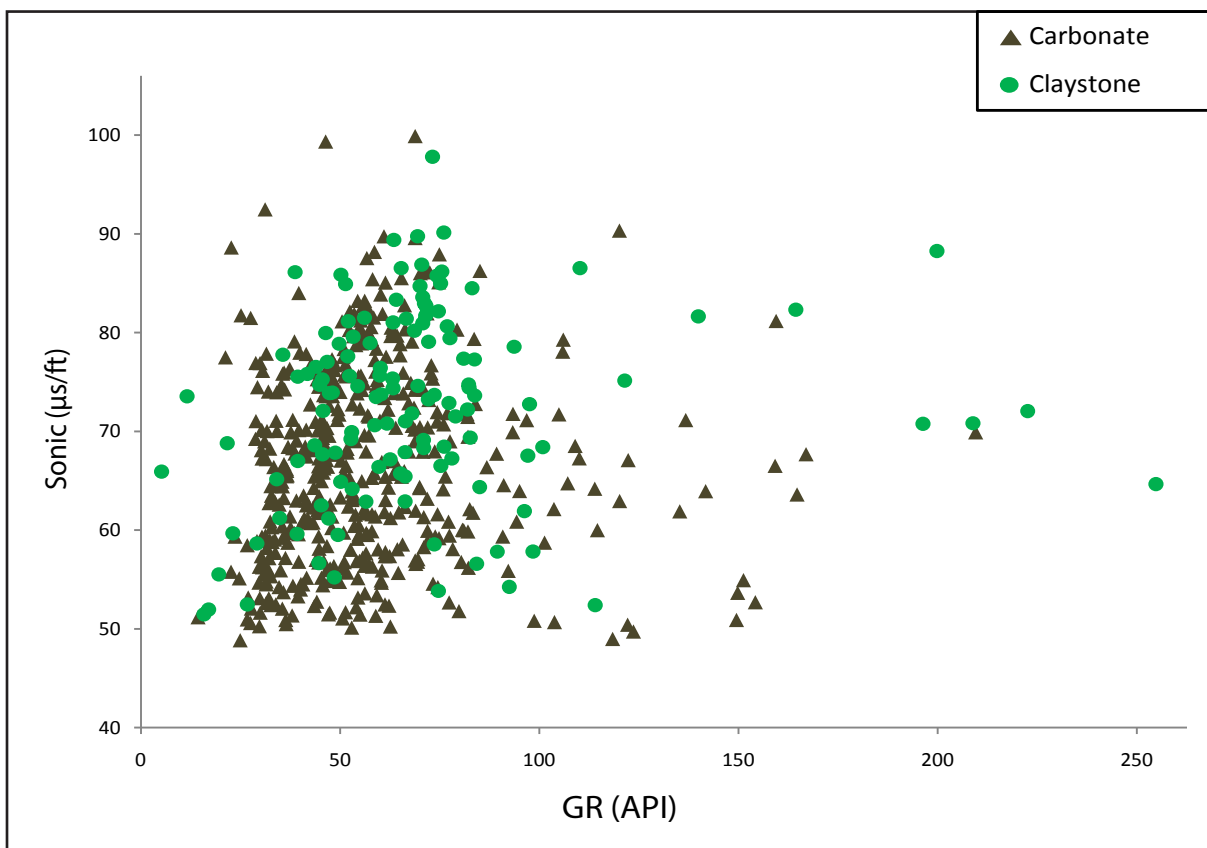


Figure 5

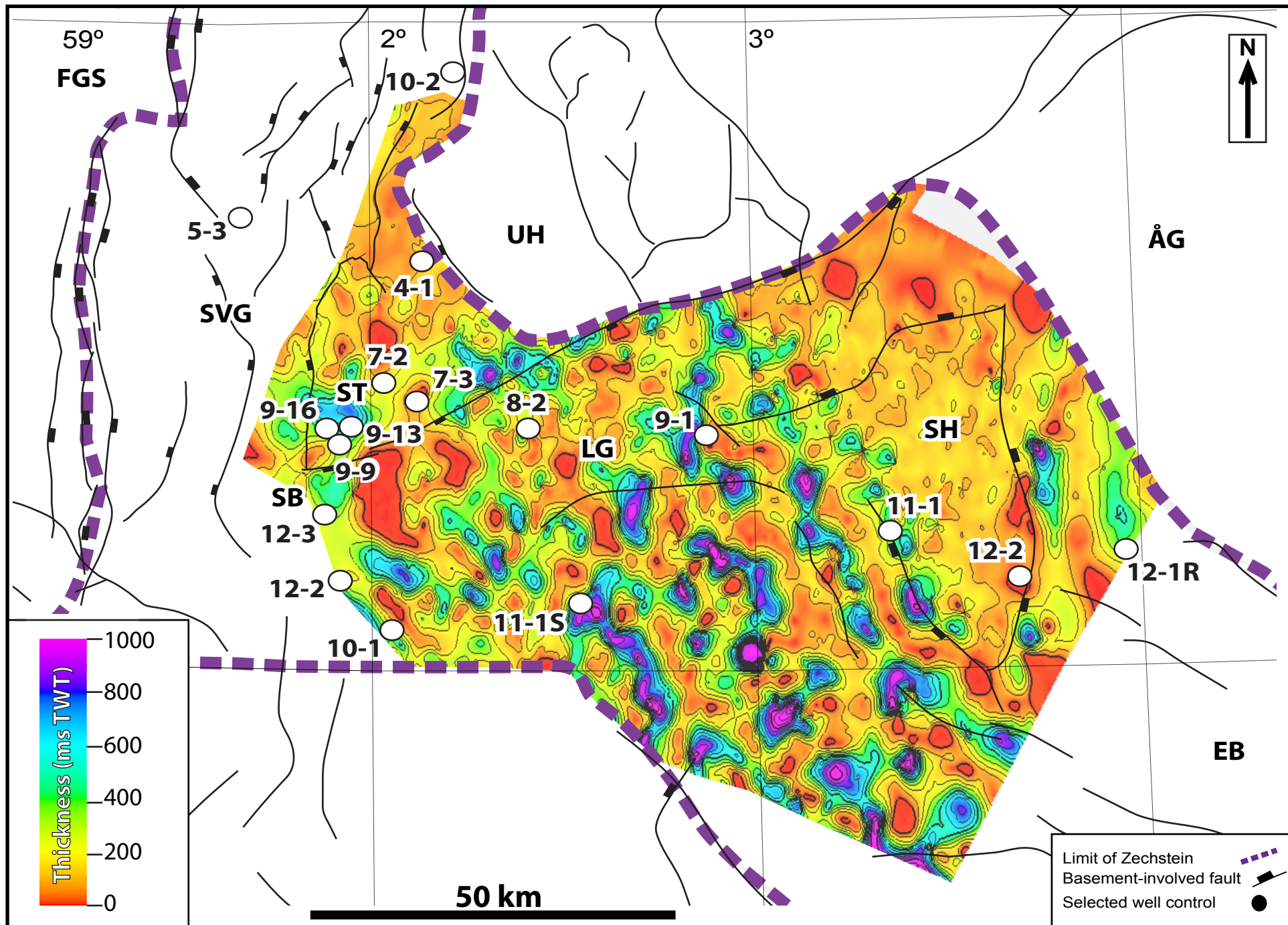


Figure 6

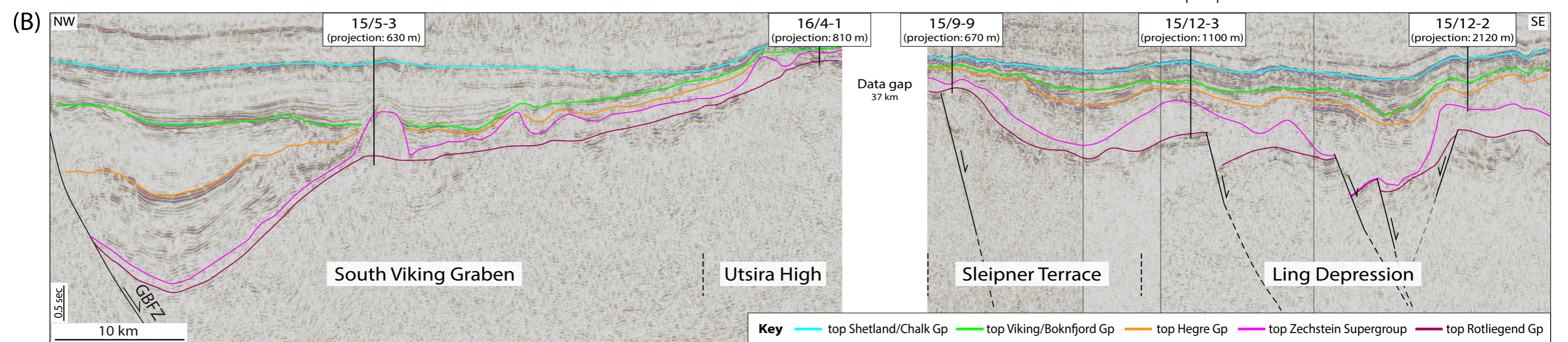
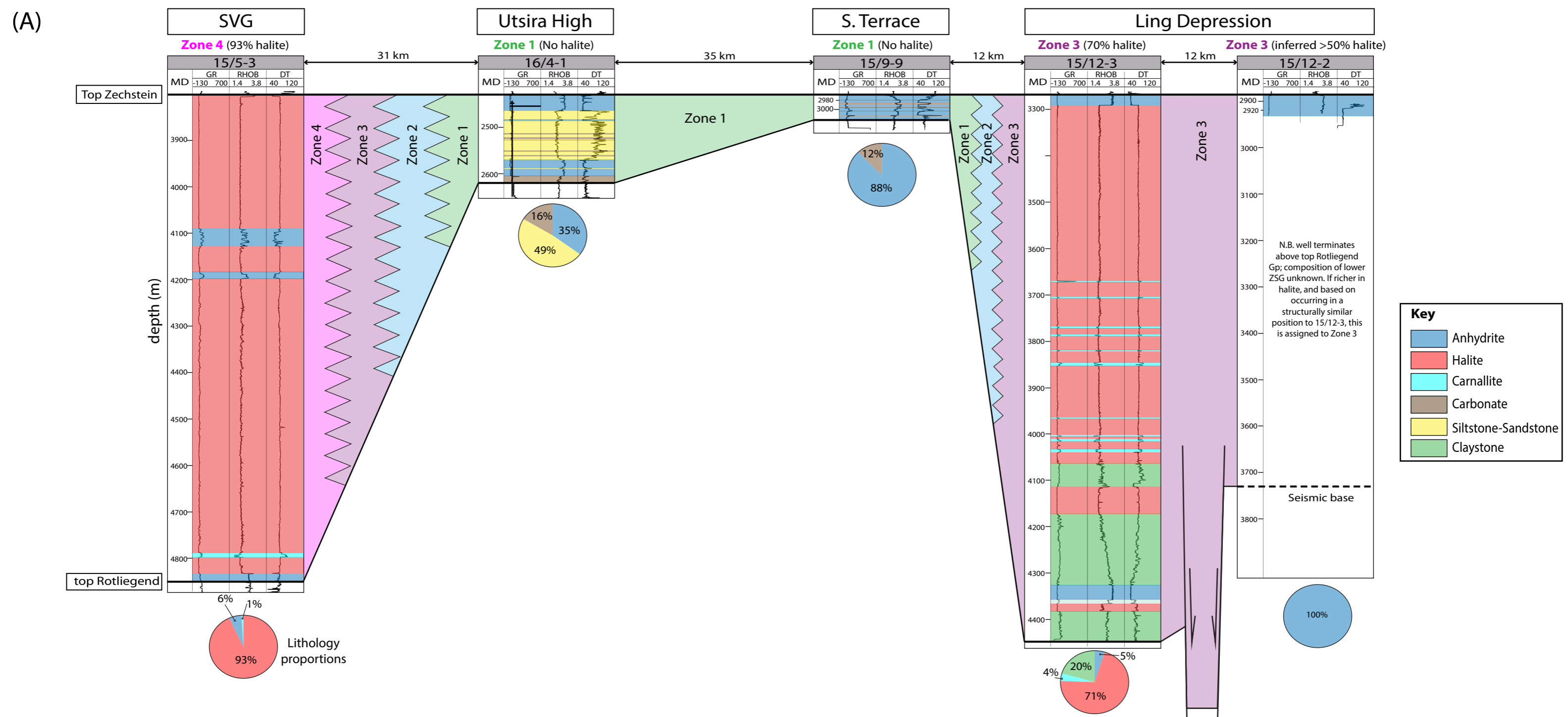


Figure 7

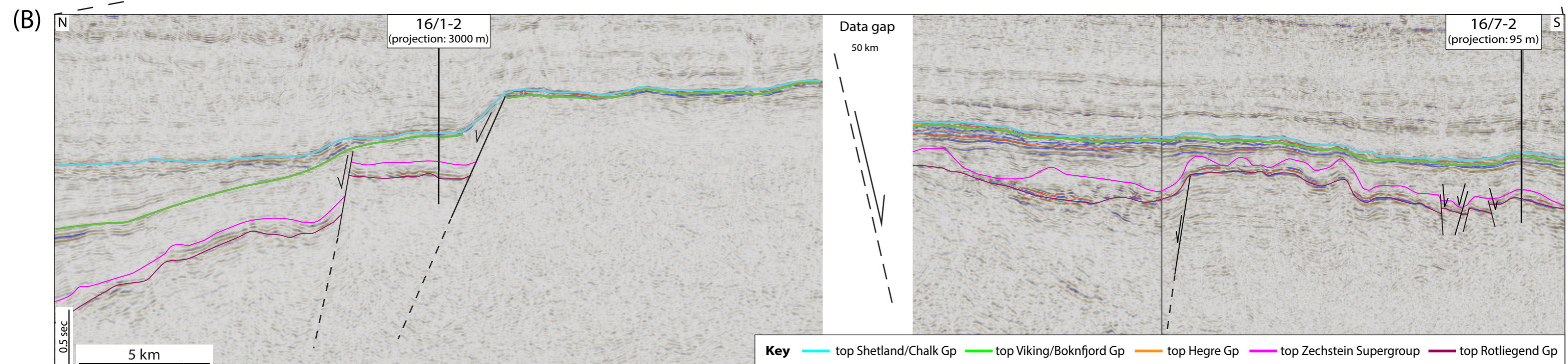
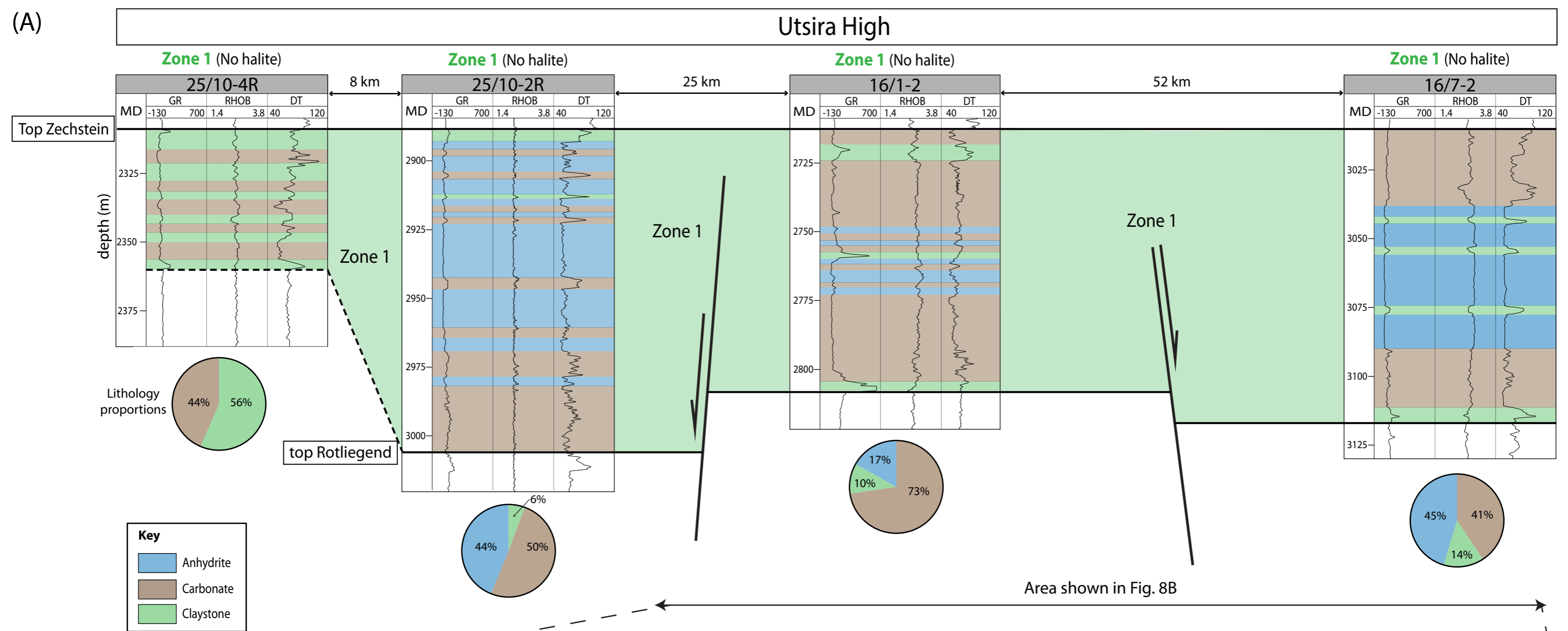


Figure 8

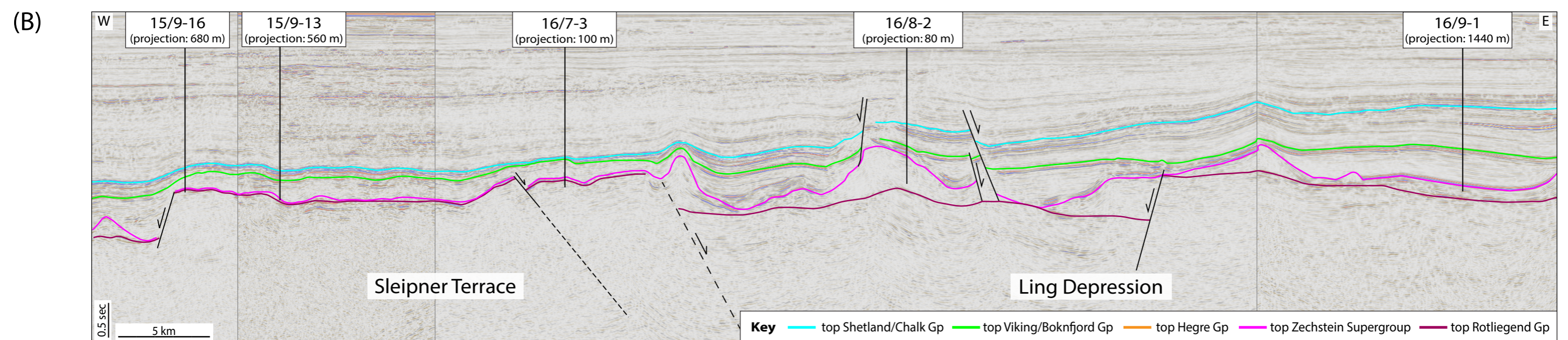
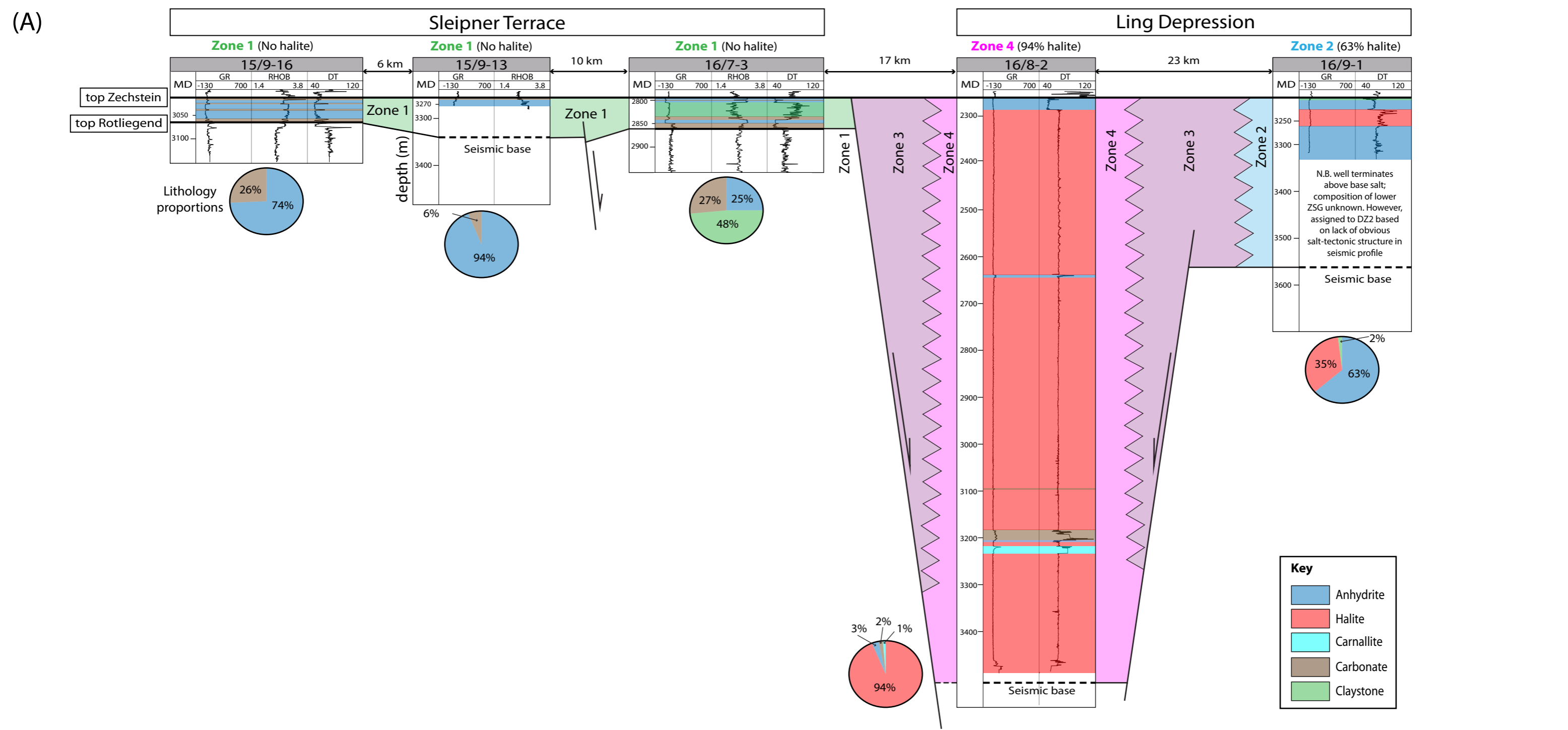


Figure 9

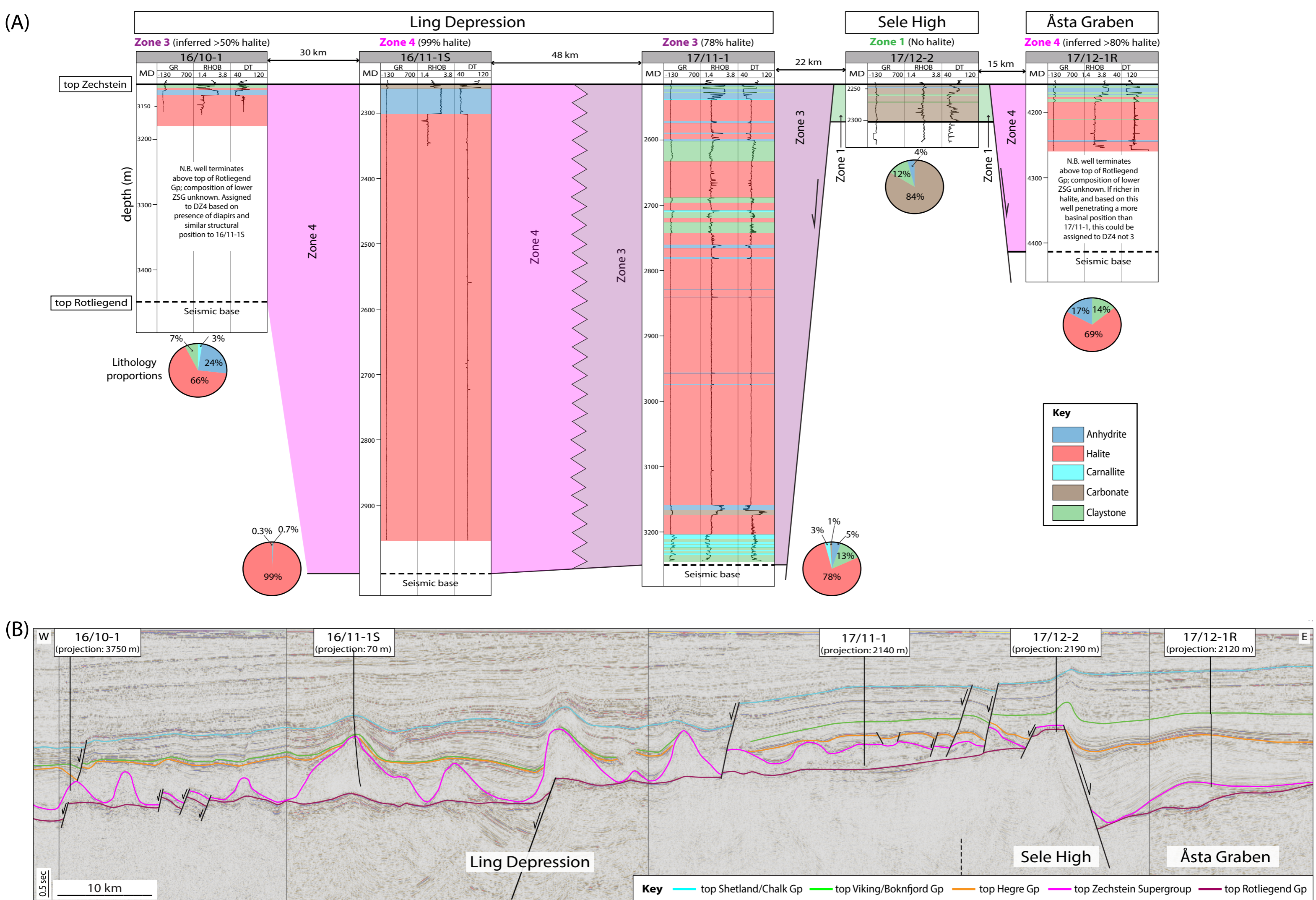


Figure 10

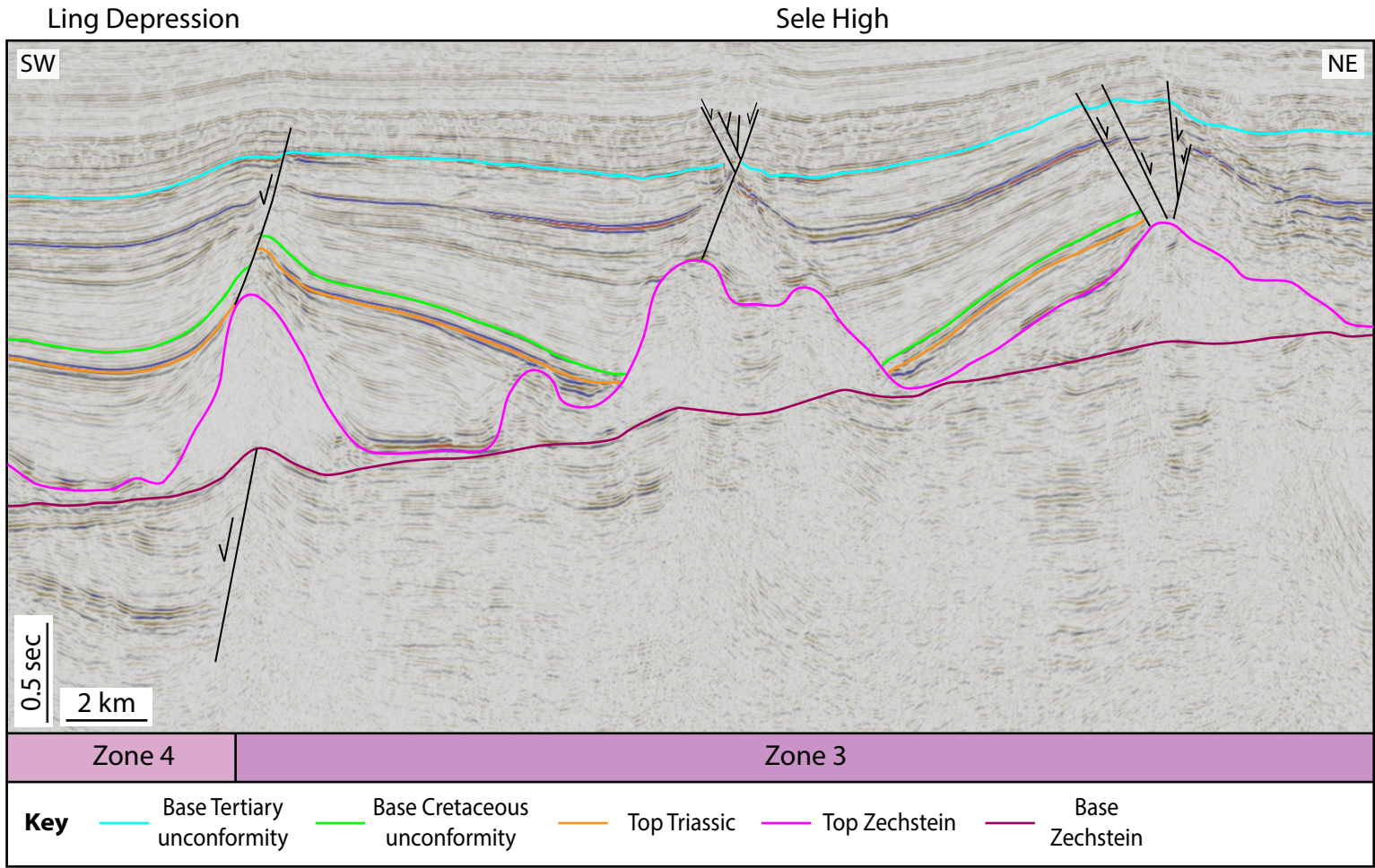


Figure 11

Ling Depression

Sele High

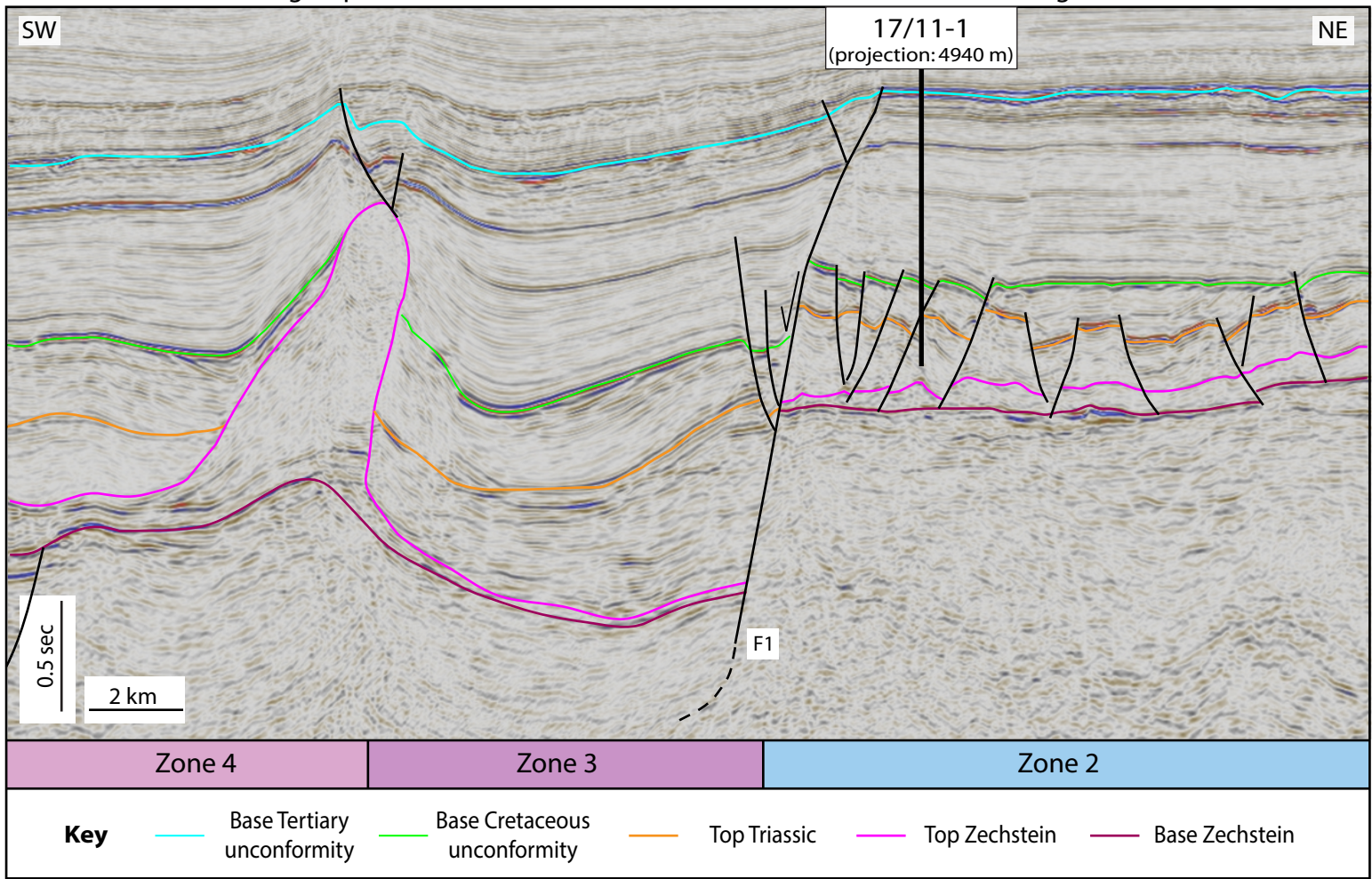


Figure 12

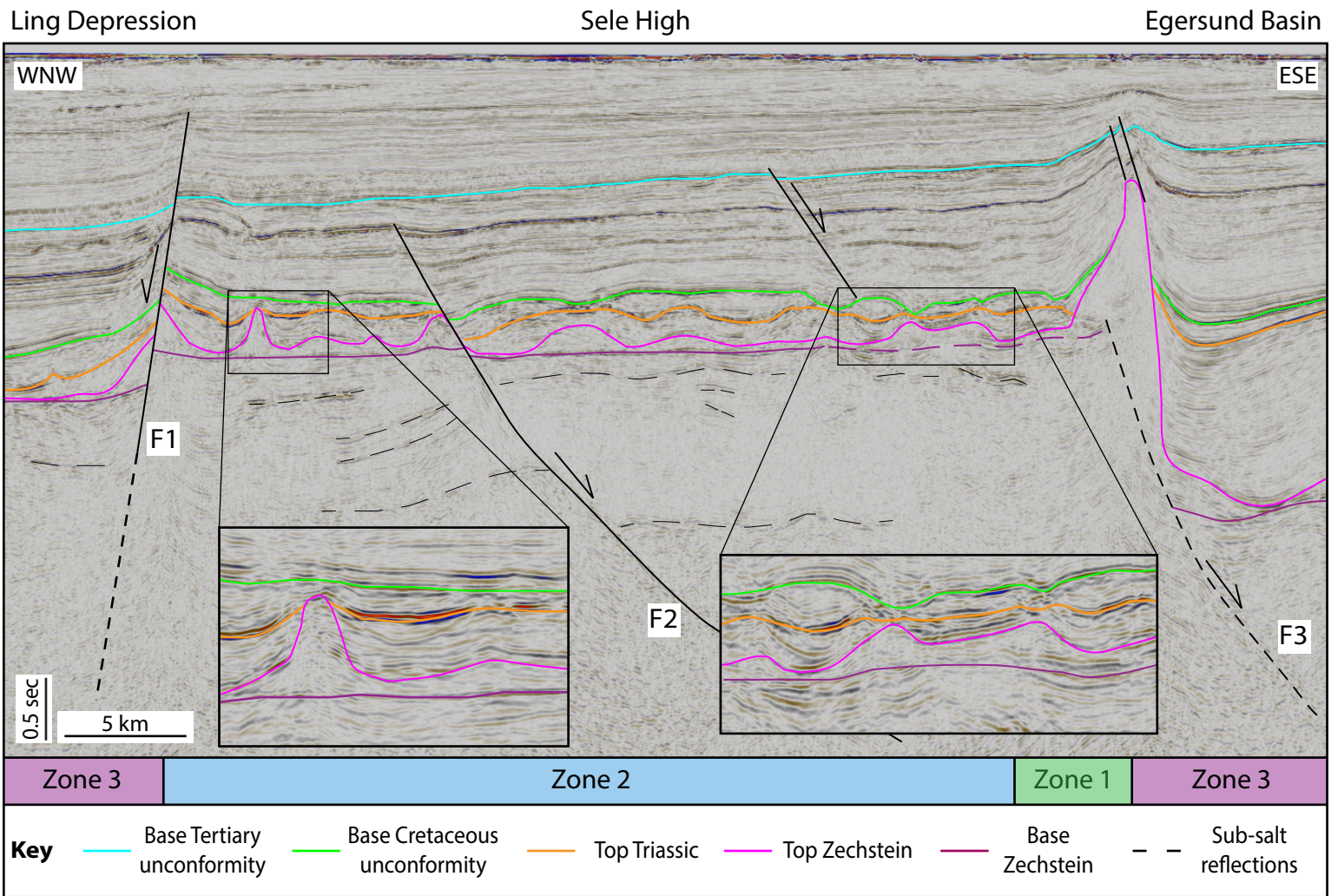


Figure 13

Lista Fault Block Complex

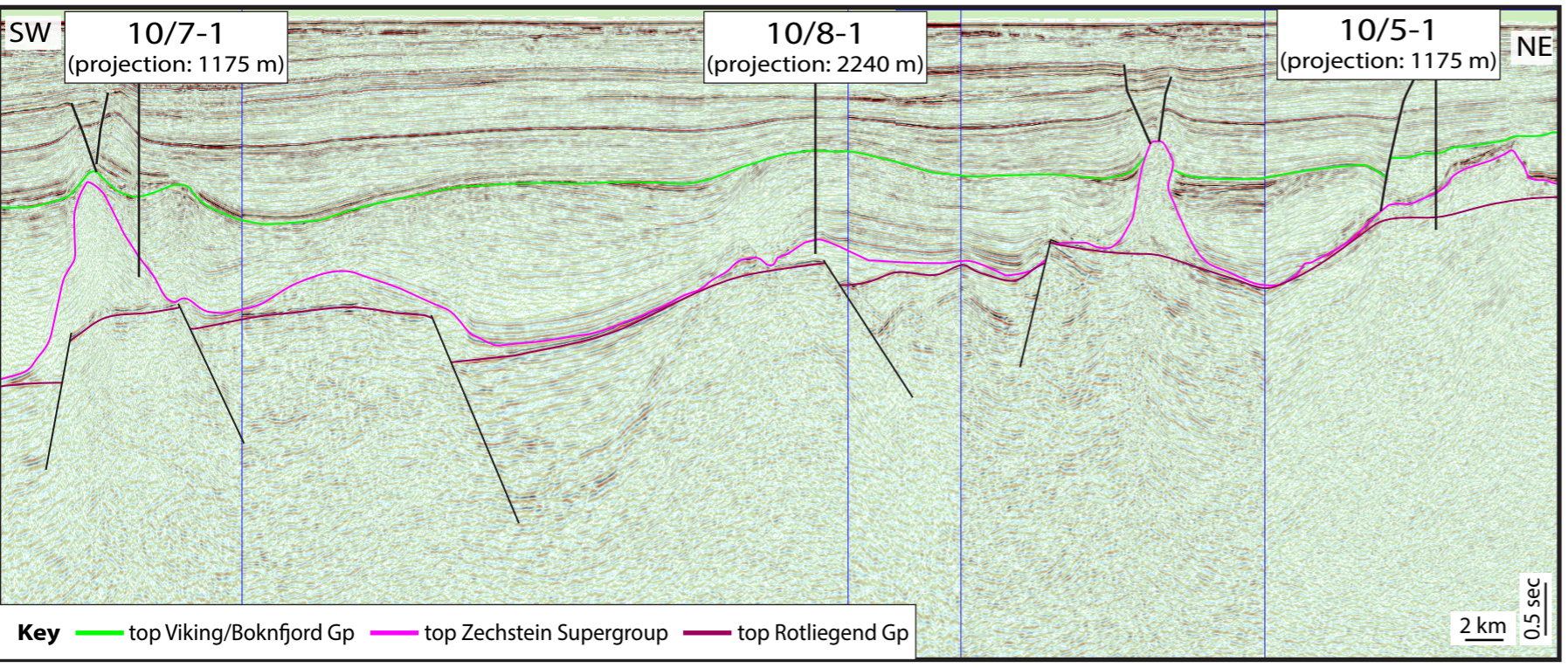
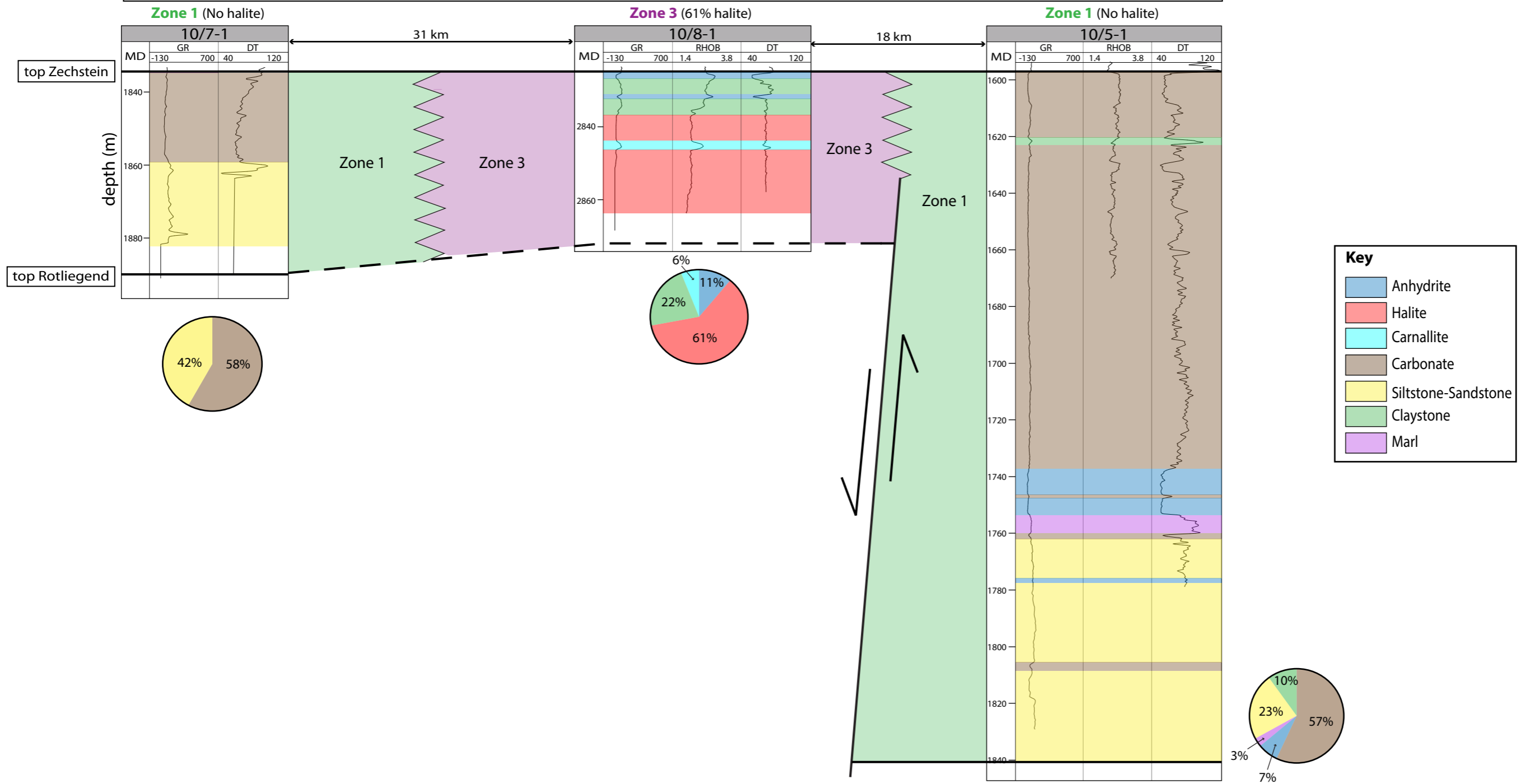


Figure 14

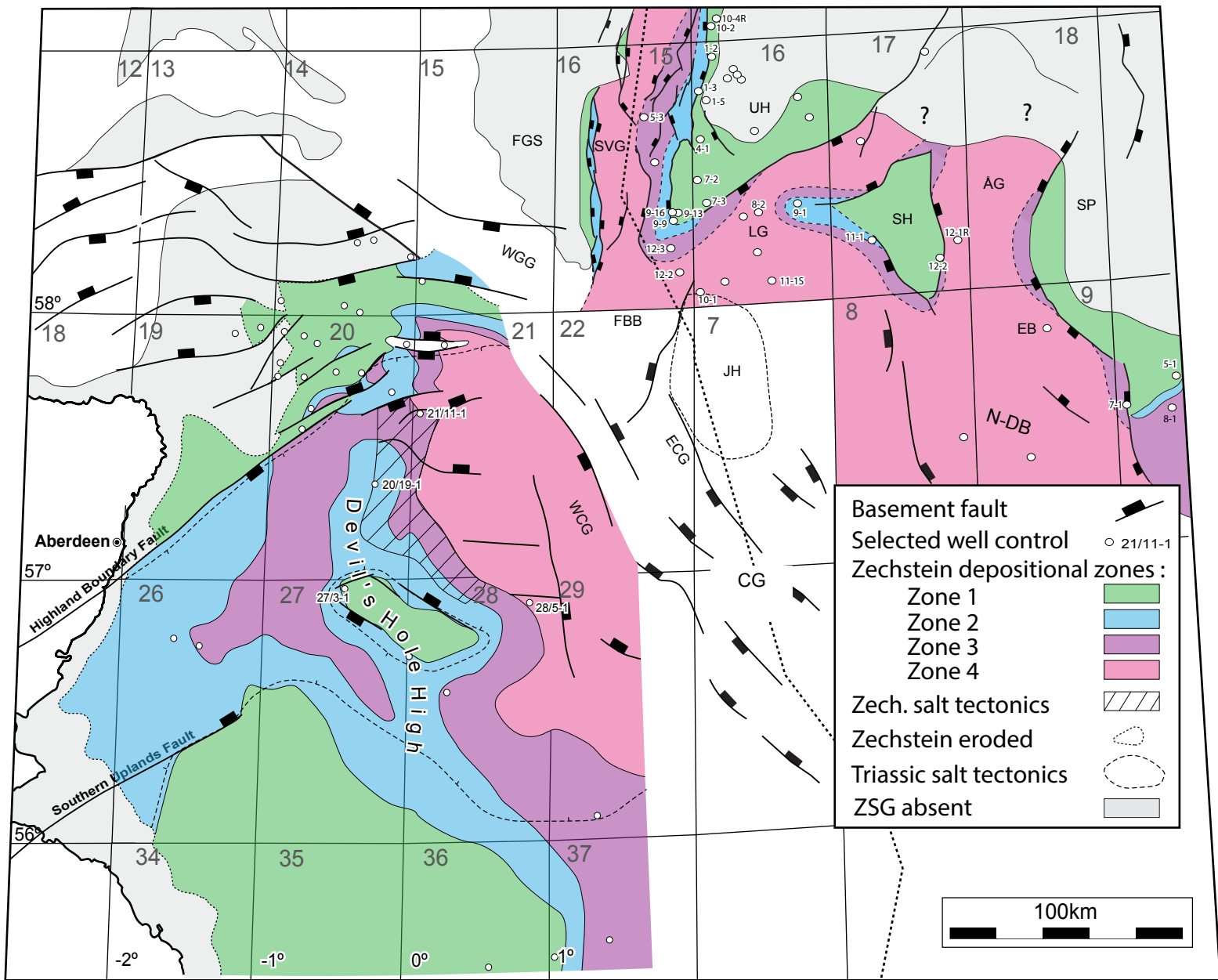
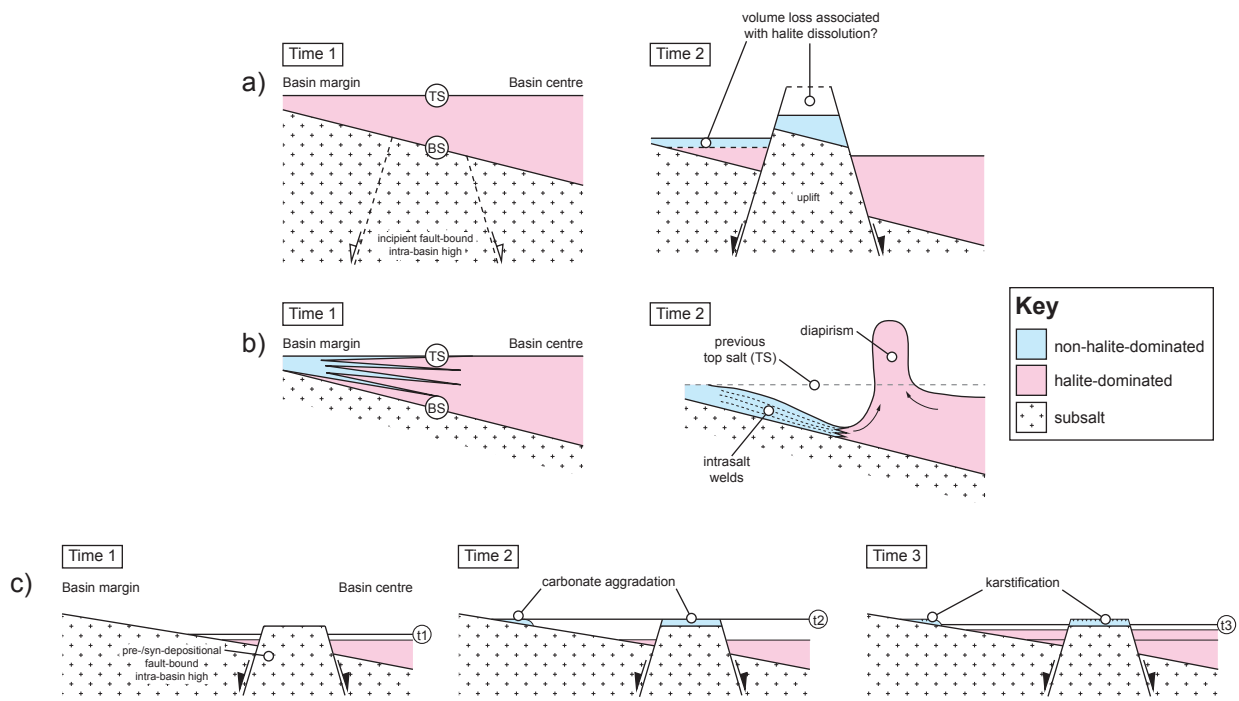


Figure 15

Fig. 16



Well name	Well-log data	TD (m)	ZSG Thickness (m)	Fully penetrate the ZSG?	Halite proportion	Inferred Depositional Zone (DZ)	Structural location	Comment
15/5-3	GR, RHOB, DT	5042	1046	Yes	93 %	4	South Viking Graben; deep basin	Penetrates off-centre of salt diapir
16/4-1	GR, RHOB, DT	2909	191	Yes	-	1	Utsira High; basin margin	Located 4 km SE of salt diapir
15/9-9	GR, RHOB, DT	3044	45	Yes	-	1	Sleipner Terrace; basin margin	
15/12-3	GR, RHOB, DT	4450	1203	Yes	71 %	3	Ling Graben; intra-basin terrace	Penetrates off-centre of salt diapir
15/12-2	GR, RHOB, DT	2924	37+	No	-	3?	Ling Graben; intra-basin terrace	Penetrates crest of salt diapir
15/9-16	GR, RHOB, DT	3120	55	Yes	-	1	Sleipner Terrace; basin margin	-
15/9-13	GR, RHOB	3280	25+	No	-	1?	Sleipner Terrace; basin margin	-
16/7-3	GR, RHOB, DT	3116	64	Yes	-	1	Sleipner Terrace; basin margin	-
16/8-2	GR, DT	3585	1325+	No	94 %	4	Ling Graben; deep basin	Penetrates off-centre of salt diapir
16/9-1	GR, DT	3340	140+	No	35 %	2?	Ling Graben; intra-basin terrace	-
25/10-4R	GR, RHOB, DT	2550	49+	No	-	1	Utsira High; basin margin	-
25/10-2R	GR, RHOB, DT	3153	126	Yes	-	1	Utsira High; basin margin	-
16/1-2	GR, RHOB, DT	2918	96	Yes	-	1	Utsira High; basin margin	-
16/7-2	GR, RHOB, DT	3146	107	Yes	-	1	Utsira High; basin margin	-
16/10-1	GR, RHOB, DT	3151	35+	No	66 %	3	Ling Graben; deep basin/intra-basin terrace	Penetrates off-centre of salt diapir crest
16/11-1S	GR, RHOB, DT	3050	794+	No	99 %	4	Ling Graben; deep basin/intra-basin terrace	Penetrates centre of salt diapir
17/11-1	GR, RHOB, DT	3270	755+	No	78 %	3	Ling Graben; intra-basin terrace	Penetrates off-centre of low-relief salt pillow
17/12-2	GR, RHOB, DT	2334	57	Yes	-	1	Sele High; basin margin	-
17/12-1R	GR, RHOB, DT	4298	165+	No	69 %	3	Egersund Basin; deep basin	Penetrates off-centre of low-relief salt pillow
10/7-1	GR, DT	1890	43	Yes	-	1	Lista Fault Block Complex; intra-basin terrace	-
10/8-1	GR, RHOB, DT	2861	36+	No	61 %	3	Lista Fault Block Complex; intra-basin terrace	Penetrates crest of salt pillow
10/5-1	GR, RHOB, DT	1842	245+	No	-	1	Lista Fault Block Complex; basin margin	Penetrates off-centre of salt diapir crest

Table 1

Table 2

Lithology	gamma-ray (GR) (API)	density (RHOB) (g/m³)	velocity (DT) (μs/ft)
carnallite	100-150 (220)	2.2.2 (1.57)	58-70 (N/A)
halite	0-30 (0)	1.9-2.3 (2.04)	65-73 (67)
anhydrite	0-70 (0-12)	2.7-3.1 (2.98)	49-58 (50)
carbonate	40-50 (12-100)	2.3-2.9 (2.85)	48-90 (44)
silt/sandstone	35-60 (0)	2.35-2.9 (2.04)	55-88 (67)
claystone	10-250 (24-1000)	1.6-2.95 (2.65-2.7)	48-90 (60-170)